Reviewed Preprint
v1 • November 21, 2025
Not revised

Reviewed Preprint
v2 • April 22, 2026
Revised by authors

Redirection of SARS-CoV-2 to Phagocytes by Intranasal sACE2-Fc as a Universal Decoy Confers Complete Prophylactic Protection

Jingyi Wang[a,†], Jiangchuan Li[a,†], Alex W Chin[b,c,†], Bin Luo[a,d], Junkang Wei[a], Jiale Qiu[a], Jianwei Ren[a,d], Yin Xia[a], Thomas Braun[a,e], Leo LM Poon[b,c,f] ✉, Bo Feng[a,d,g] ✉

[a]School of Biomedical Sciences, Faculty of Medicine; GIBH CAS-CUHK Joint Research Laboratory on Stem Cell and Regenerative Medicine, The Chinese University of Hong Kong, Hong Kong SAR, China • [b]School of Public Health, LKS Faculty of Medicine, The University of Hong Kong, Hong Kong SAR, China • [c]Centre for Immunology & Infection, Hong Kong Science and Technology Park, Hong Kong SAR, China • [d]Centre for Regenerative Medicine and Health, Hong Kong Institute of Science & Innovation, Chinese Academy of Sciences, Hong Kong SAR, China • [e]Department of Cardiac Development and Remodeling, Max-Planck-Institute for Heart and Lung Research, Bad Nauheim, Germany • [f]HKU-Pasteur Research Pole, LKS Faculty of Medicine, The University of Hong Kong, Hong Kong SAR, China • [g]Guangzhou Institutes of Biomedicine and Health, Chinese Academy of Sciences, Guangzhou, China

✉ **For correspondence:**
llmpoon@hku.hk
fengbo@cuhk.edu.hk

† These authors contribute equally.

Competing interests: No competing interests declared

Funding: See page 33

Reviewing editor: Bavesh D Kana, University of the Witwatersrand, South Africa

eLife Assessment

This manuscript presents a **valuable** antiviral approach using an engineered ACE2-Fc fusion protein that demonstrates broad-spectrum neutralization capacity against SARS-CoV-2 variants and achieves significant prophylactic protection in animal models through a novel Fc-mediated phagocytosis mechanism. The study provides **convincing** evidence for protective efficacy through rigorous in vivo validation in mice, mechanistic characterization via biodistribution studies and macrophage depletion assays, and demonstration of antibody-dependent cellular phagocytosis as the primary clearance mechanism. The work will be of interest to researchers working in vaccine development and associated immune responses.

https://doi.org/10.7554/eLife.108883.2.sa4

Abstract

The rapid evolution of SARS-CoV-2 and other respiratory RNA viruses limits the success of current vaccines and antibody-based therapies. Engineered decoy receptors based on soluble angiotensin-converting enzyme 2 (sACE2) offer promising alternatives. Clinical-grade recombinant sACE2 inhibits SARS-CoV-2 replication *in vitro* but shows limited clinical success. This study reports an optimized sACE2 mutant fused to human IgG1 Fc (B5-D3), which redirects virus–decoy complexes to lysosomal degradation in macrophages. Intranasal prophylactic delivery of B5-D3 confers complete protection in SARS-CoV-2-infected K18-hACE2 mice. Abrogation of Fc effector functions compromises antiviral protection, indicating that Fc-mediated uptake of virus–decoy complexes is critical. Transcriptomic analysis suggests that B5-D3 induces early immune activation in lungs of infected mice. Bio-distribution and flow cytometry reveal selective targeting of airway phagocytes. *In vitro* assays confirm lysosomal degradation of virus–decoy complexes by macrophages without productive infection. These findings reveal a distinct antiviral mechanism via phagocytic clearance, supporting refined regimens for decoy treatments against SARS-CoV-2 and potentially other respiratory viruses.

Introduction

The incessant evolution of severe acute respiratory syndrome coronavirus 2 (SARS-CoV-2) and frequent breakthrough infections during the coronavirus disease 2019 (COVID-19) pandemic underscore the critical need for effective antiviral strategies that are less susceptible to immune escape than conventional vaccines and monoclonal antibody (mAb) therapies [1].

Soluble angiotensin-converting enzyme 2 (sACE2) therapies, which employ recombinant forms of the human angiotensin-converting enzyme 2 (ACE2) receptor—the primary binding site for the SARS-CoV-2 spike protein [1–5]—as viral decoys, have emerged as a promising alternative [6]. However, an early clinical version (amino acid [aa] 1-740, APN01) showed limited therapeutic benefit [7] and raised safety concerns about interference with endogenous renin-angiotensin system (RAS) [8]. Subsequent protein engineering greatly improved the pharmacological properties of sACE2, including fusion with a human IgG1 Fc domain (sACE2-Fc) to enhance serum half-life [9], and mutagenesis to enhance spike-binding affinity [10–12] and abolish enzymatic activity [10, 12, 13]. Potent sACE2-Fc mutants have shown broad-spectrum neutralization against SARS-CoV-2 variants in animal models [14–16]. However, their efficacy in protecting hosts from viral infections was often incomplete. Despite the evidence suggesting a role for Fc-mediated effector functions in sACE2-Fc efficacies [14], underlying immune mechanisms remained poorly understood. Further investigation that systematically assesses the potential to optimize decoy design, strategies of administration, and mechanisms of actions is pivotal to the development of ACE2 decoy-based antivirals and harnessing their full potential.

In this study, we engineered a potent yet minimally mutated sACE2-Fc decoy candidate (B5-D3) with just two mutations to enhance spike-binding (T92Q) while eliminating enzymatic activity (H374N). Broad-spectrum neutralization capacity against multiple SARS-CoV-2 variants was confirmed by *in vitro* neutralization assays. Markedly, stepwise examinations of various administration routes and time points identified intranasal (IN) prophylaxis as the most effective regimen for B5-D3, which conferred complete protection against SARS-CoV-2 infection in K18-hACE2 mice across age groups. Whereas B5-D3 intravenously administered either prior or post infection, showed activity that moderately improved disease outcome. To understand how sACE2-Fc decoys influence viral fate and achieve superior antiviral protection via IN prophylaxis, we carried out systematic, mechanistic investigations through transcriptomics, bio-distribution, and phagocytosis analysis. Our results revealed that IN-delivered B5-D3 engages airway phagocytes to promote early viral clearance and host immune activation, which uncovers a distinct antiviral mechanism and offers a universal and commonly applicable “decoy strategy” to combat unknown air-borne respiratory virus in the future.

Results

Engineered sACE2-Fc decoys with two single mutations achieve robust neutralization against SARS-CoV-2 variants

To generate representative ACE2 decoys with optimal performance, we adopted the established sACE2-Fc fusion design [9] (Fig. 1a; Supplementary Fig. 1) and selectively verified mutation(s) proposed in prior studies, either to enhance the binding of human ACE2 to SARS-CoV-2 spikes [17] (B2–B6) or to abolish enzymatic activity [10–12, 18] (A2, A3, D1–D5) (Supplementary Fig. 2a,b). The sACE2-Fc candidates generated with either type of mutation(s) were all verified for pseudovirus-based neutralization assays [19] and ACE2 enzymatic activity. Indeed, mutants B2–B6 showed consistently enhanced neutralization capacity against both Wuhan-Hu-1 and D614G pseudoviruses [20] (Fig. 1b; Supplementary Fig. 2c,d). Notably, B5 with the single T92Q mutation, which increases spike affinity by removing a critical glycosylation site at N90 [21], exhibited remarkable neutralization enhancement among other multi-mutants. Meanwhile, mutations selected for catalytic inactivation, including the previously reported mutation pairs A2 [11, 18], A3 [10], single mutations derived from these pairs (D1, D3, D4, but not D2), and a recently reported single mutation D5 [12], effectively abolished enzymatic activity while showing minimal

effect on spike binding (Fig. 1b; Supplementary Fig. 2e). We next combined the B5 (T92Q) mutation with each of the inactivating mutations. Notably, among the resulting compound mutants, B5-D1, B5-D3, B5-D4, and B5-D5 with two mutations remained to be enzymatically inactive while retaining comparable or stronger neutralization capacity than B5-A2 and B5-A3 with three mutations (Fig. 1b; Supplementary Fig. 2f–h). B5-D3 (T92Q/H374N) emerged as one of the best candidates (Fig. 1a, red stars; Fig. 1b, red arrow), exhibiting minimal deviation from wild type (WT) ACE2 in structural modeling (root mean square deviation [RMSD] = 0.212 Å; Supplementary Fig. 2i) [22].

To assess the breadth of neutralization, we tested three double mutants (B5-D3, B5-D4, and B5-D5) against pseudoviruses bearing spikes from various variants of concern (VOCs) and variants of interest (VOIs) [1, 23–27]. All three designs showed dose-dependent neutralization with higher potency than WT sACE2-Fc (Fig. 1c,d; Supplementary Fig. 3). We further examined B5-D3, as a representative decoy candidate, against authentic SARS-CoV-2 using plaque reduction neutralization tests (PRNTs) in Vero E6 cells, which indeed, confirmed its robust activity against Wuhan-Hu-1, Delta, and Omicron variants BA.5, BQ.1.22, and XBB.1.5 strains [1, 24, 28, 29] (Fig. 1e-g). In contrast, Casirivimab, serving as positive control [30], showed efficacy only against early variants (Wuhan-Hu-1 and Delta; Fig. 1f), but failed to neutralize Omicron sublineages (Fig. 1g). These results demonstrate that a rationally engineered sACE2-Fc decoy with only two mutations could achieve potent and safe neutralization across SARS-CoV-2 variants, reducing the potential risks associated with extensive mutagenesis.

Prolonged *in vivo* overexpression of sACE2-Fc double mutants demonstrates minimal RAS disturbance and no tissue damage in mice

Next, we evaluated the safety of the sACE2-Fc double mutants *in vivo* (Supplementary Fig. 4a). Adult K18-hACE2 transgenic mice with immune tolerance to human ACE2 [31] were intravenously injected with adenovirus-associated virus (AAV) vectors encoding either WT sACE2-Fc or double mutants at a dose of 1×10^{11} genome copies (GC) per mouse. Notably, serum levels of the double mutants (B5-D3, B5-D4, and B5-D5) were significantly higher than those of WT sACE2-Fc (Supplementary Fig. 4b; Supplementary Table 1). This trend was further supported by quantification of AAV genomes in the liver, indicating greater *in vivo* stability or tolerance of the double mutants (Supplementary Fig. 4c).

Importantly, despite prolonged high-level expression, ELISA measurements of serum renin, Angiotensin II (Ang II), and Ang (1–7) [8] demonstrated minimal disturbance to the RAS in mice treated with the double mutants (Supplementary Fig. 4d–f). In contrast, WT sACE2-Fc treatment led to significantly elevated serum levels of renin and Ang II, indicating a disruption of the RAS (Supplementary Fig. 4d,e). Histological examination of multiple organs at the end point showed no evidence of tissue damage in any of these groups (Supplementary Fig. 4g). These observations collectively underscore the improved safety of catalytically inactive sACE2-Fc mutants, supporting their suitability for prolonged or repeated use.

Prophylactic administration of the sACE2-Fc B5-D3 mutant via the intranasal route exhibits superior protection against SARS-CoV-2

Next, we evaluated the *in vivo* efficacy of the sACE2-Fc double mutant B5-D3 against SARS-CoV-2 infection using aged K18-hACE2 mice (10 – 12 months old) (Fig. 2a). 6 hours (h) before inoculating with 1×10^4 plaque-forming unit (PFU) of SARS-CoV-2 (Wuhan-Hu-1 strain), mice received a prophylactic dose of recombinant B5-D3 protein either intranasally (IN, 2.5 mg/kg) or intravenously (IV, 15 mg/kg). To simulate a therapeutic intervention, an additional group received IV B5-D3 (15 mg/kg) 24 h post-virus inoculation. The vehicle control group received an intranasal PBS administration 6 h before viral challenge. Over a 14-day observation period, all mice in the PBS group exhibited significant weight loss and succumbed to infection by 7 days post-infection (dpi) (Fig. 2b,c, black lines). Both IV-treated groups exhibited initial weight loss similar to the

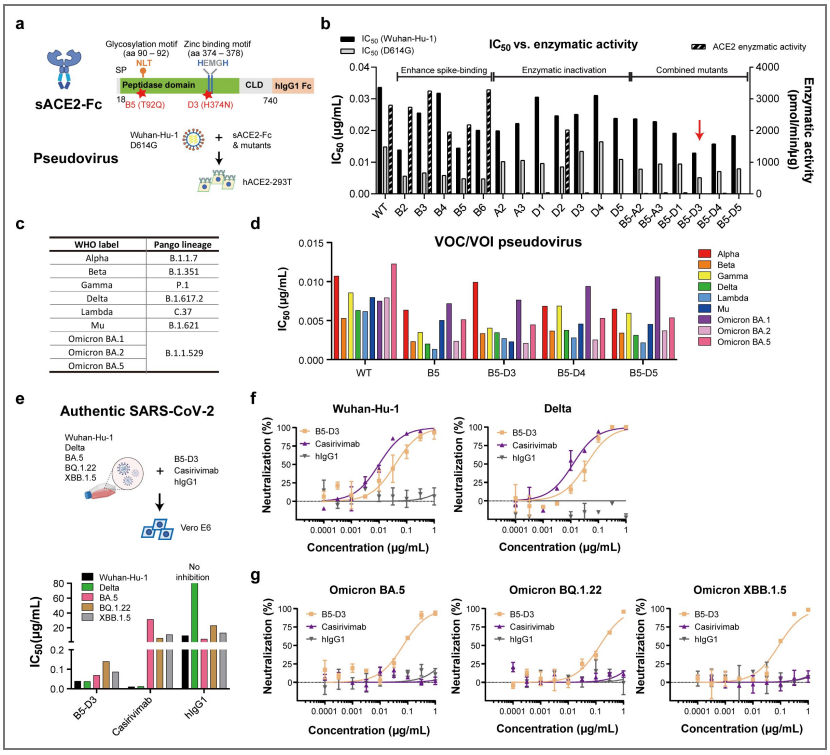

Fig. 1. Enhanced sACE2-Fc with two single mutations exhibited broad-spectrum neutralization of SARS-CoV-2 variants.

a Schematic representation of sACE2-Fc structure (upper) and neutralization assay setup (lower). Key amino acid positions (90-92 and 374-378) involved in glycosylation and zinc binding are highlighted. Red stars mark the positions of mutations in the sACE2-Fc mutant B5-D3. SP, signal peptide; CLD, collectrin-like domain; hIgG1, human IgG1. **b** Comparative bar graph showing the half-maximal inhibitory concentration (IC_{50}) values for neutralization of Wuhan-Hu-1 and D614G pseudovirues by WT sACE2-Fc and mutants (B2 to B6, A2, A3, D1 to D5, and B5-derivatives). The red arrow emphasizes the superior performance of the B5-D3 mutant. Enzymatic activity of each construct is plotted on the right axis. **c** List of pseudoviruses carrying spikes from different SARS-CoV-2 variants tested, categorized by the World Health Organization (WHO) into VOCs and VOIs. **d** Graph displaying IC_{50} values of WT sACE2-Fc, B5, and B5-D3/4/5 mutants against various SARS-CoV-2 VOCs and VOIs in neutralization assays. **e** Schematics of the plaque-reduction neutralization tests (PRNTs) process (upper) and the resulting IC_{50} values for B5-D3, Casirivimab, and hIgG1 against authentic SARS-CoV-2 (lower). **f, g** Dose-response curves depicting the neutralization efficacy of B5-D3 (orange), Casirivimab (purple), and hIgG1 (grey) in PRNTs against authentic SARS-CoV-2 Wuhan-Hu-1 and Delta strains (**f**), and Omicron sub-lineages (**g**). Data are presented as mean ± standard deviation (SD) from duplicate experiments.

PBS group; however, two out of four mice in each group began to regain weight from 10 dpi and survived until the observation endpoint, suggesting improvement in disease severity and survival (green and blue lines). Notably, all mice in the IN-prophylaxis group, despite receiving a 6-fold lower dose of B5-D3 protein than those in the IV groups, maintained stable body weight and achieved complete survival over the 14-day period (red lines).

To monitor viral burden, one mouse from each group was sacrificed at 4 dpi (Fig. 2a). Corroborating the body weight and survival data, no infectious viral particles were detected in lung homogenate from the IN-prophylaxis mouse. In contrast, mice treated with IV prophylaxis or therapy showed reduced but still detectable viral titers compared to the PBS group (Fig. 2d). Immunohistochemistry (IHC) staining further confirmed the absence of viral nucleocapsid (N) protein in the IN-treated mouse, whereas IV-treated mice showed residual infection and immune cell infiltration. H&E staining revealed varying degrees of alveolar thickening in all SARS-CoV-2-inoculated mice (Fig. 2e).

To further explore the effective timing of IN administration that offers superior antiviral protection, we treated a younger cohort of K18-hACE2 mice (2 – 3 months old) with B5-D3 (IN, 2.5 mg/kg) at –24 h, –6 h, or +24 h relative to viral challenge (Fig. 2f). Consistently, all mice in the PBS group of the young cohort exhibited substantial weight reduction from 4 dpi and reached approximately 20% loss by 7 dpi (Fig. 2g, black lines). Whereas differently from the aged cohort, two of the five infected young mice eventually recovered, resulting in 40% survival (Fig. 2g,h, black lines) indicating age-related fitness [32]. Interestingly, both the –24 h and –6 h IN-prophylaxis groups maintained stable body weights (Fig. 2g, pink and red lines), ending up with survival rates of 80% and 100%, respectively (Fig. 2h). In contrast, the +24 h IN-therapy group showed substantial weight loss and no survival improvement compared to the PBS group, indicating that high-efficiency antiviral protection of IN B5-D3 is limited to prophylactic administration but not post-infection treatments (Fig. 2g,h, orange lines). Consistently, virus-neutralizing antibodies were detected in surviving mice from the PBS and +24 h groups at 14 dpi, indicating once active infection and subsequent immune response. Whereas antibody levels remained minimal in the two IN-prophylaxis groups, suggesting effective prevention of viral replication (Fig. 2i).

Efficient protection against SARS-CoV-2 by intranasal B5-D3 prophylaxis depends on Fc-mediated effector functions

Adding on to the 2-week observation of the significant protection conferred by IN prophylaxis with B5-D3, we examined the early responses following SARS-CoV-2 challenge in K18-hACE2 mice. A new cohort of 2- to 3-month-old mice received B5-D3 IN treatment 6 h before infection (–6 h), and lung tissues were harvested at 1, 2, and 4 dpi for analysis (Fig. 3a). An additional group was treated with a modified version of B5-D3, which contains L234A/L235A mutations in the human IgG1 Fc region (B5-D3-LALA) to abolish its binding to Fc gamma receptor (FcγR) and abrogate Fc effector functions [33] (Supplementary Fig. 5). Quantitative PCR of viral spike (*S*) and nucleocapsid (*N*) RNA in lung tissues revealed only marginal viral loads in the B5-D3-treated mice at as early as 1 dpi, indicating efficient suppression of early viral replication compared to the PBS group (Fig. 3b). Analysis of infectious viral particles in lung homogenates further corroborated these observations, demonstrating minimal or undetectable viral titers in the B5-D3 group at all time points (Fig. 3c). In contrast, PBS-treated mice exhibited consistently high viral loads. Interestingly, the analysis of B5-D3-LALA group detected varied levels of *S* and *N* RNAs and significant viral burdens in two out of three mice, indicating partial protection and supporting that Fc effector functions are indispensable for full efficacy of IN B5-D3 (Fig. 3b,c, right panels). Consistently, IHC staining for N protein in lung sections confirmed the absence of viral infection in the B5-D3 groups at all time points. Whereas signs of viral replication were evident in the lungs of mice treated with PBS since as early as 1 dpi and in the B5-D3-LALA-treated cohort as examined at 4 dpi (Fig. 3d; Supplementary Fig. 6, left panels). Despite variations in viral burden, H&E staining indicated alveolar septal thickening in all groups (Fig. 3e; Supplementary Fig. 6, right panels; Supplementary Fig. 7). Notably, moderate alveolar thickening persisted in the B5-D3-treated mice till the end point at 4 dpi, whereas the PBS groups developed much severer alveolar

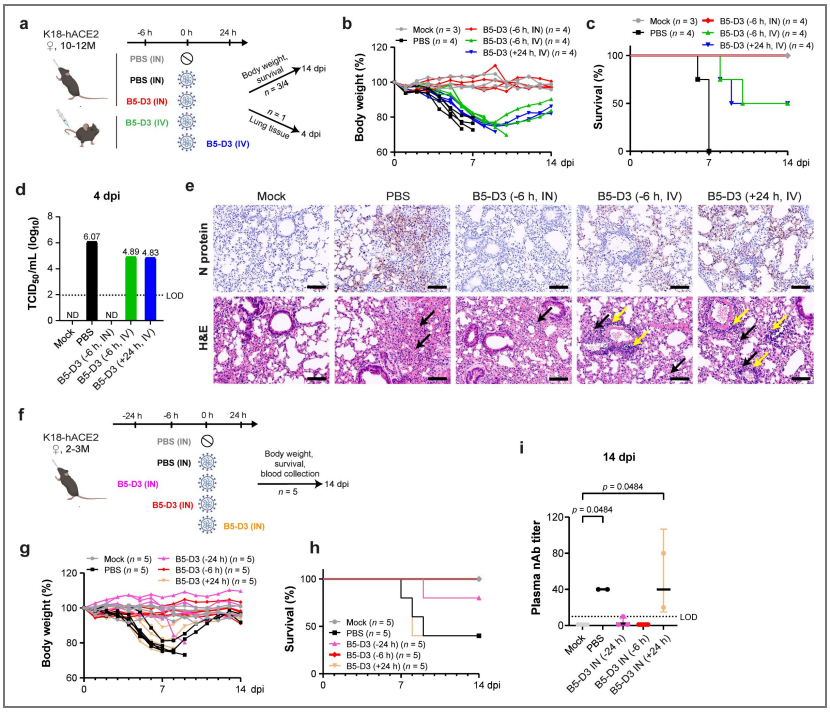

Fig. 2. Enhanced survival and reduced infection in K18-hACE2 mice through intranasal prophylaxis with B5-D3 against SARS-CoV-2.

a–e Female K18-hACE2 mice, aged 10 to 12 months, were inoculated with 1 × 10^4 PFU of SARS-CoV-2 (Wuhan-Hu-1 strain). Mice were treated with B5-D3 6 h prior (−6 h) via intranasal (IN, red) or intravenous (IV, green) routes, or 24 h post-infection (+24 h, blue) via IV (n = 4 + 1). IN PBS administered 6 h prior to viral challenge served as the vehicle control (black; n = 4 + 1), and PBS alone was used for mock control (grey; n = 3 + 1) (**a**). Body weight and survival (n = 3 or 4) were monitored over 14 days (**b**, **c**). One mouse from each group was sacrificed at 4 dpi for analysis of viral titers in lung homogenates using a median tissue culture infectious dose ($TCID_{50}$) assay (**d**) and histological analysis of lung sections (upper, IHC staining for N protein; lower, H&E staining) (**e**). Black arrows indicate alveolar thickening, and yellow arrows show leukocyte infiltration. Scale bar = 100 μm. ND, not detected; LOD, limit of detection. **f–i** Young female K18-hACE2 mice, aged 2 to 3 months, were inoculated similarly and treated with B5-D3 via IN route at 24 h before (−24 h, pink), 6 h before (−6 h, red), or 24 h after (+24 h, orange) the viral challenge (n = 5). Mice receiving IN PBS 6 h before infection served as the vehicle control (black), with mock control mice receiving PBS alone (grey) (**f**). Body weight (**g**) and survival (**h**) were recorded for 14 days. Neutralizing antibody titers against Wuhan-Hu-1 in serum samples from surviving mice at 14 dpi were determined using Vero E6 cells (**i**). nAb, neutralizing antibody. Data are presented as the geometric mean ± geometric SD. Statistical significance was determined using Dunn's multiple comparisons test.

thickening at 4 dpi. Consistent with the partial protection observed with B5-D3-LALA, histological analysis of lung samples in this group revealed severer yet heterogenous alveolar thickening (Supplementary Fig. 7). These findings collectively demonstrated that IN prophylaxis with B5-D3 blocks SARS-CoV-2 infection not only by neutralization but also by immune mechanisms such as Fc-mediated effector functions.

RNA-Seq analysis of lung transcriptomes reveals early antigen presentation and prompt viral clearance following SARS-CoV-2 neutralization by B5-D3

To delineate the immune mechanisms underlying IN B5-D3-mediated prophylactic protection against SARS-CoV-2, we examined the transcriptomes of lung samples collected at 1, 2, and 4 dpi from the above experiment (Fig. 4a–d; Supplementary Fig. 8a). Unsupervised clustering based on Pearson correlation distinguished samples with severe infection (mainly PBS-treated) from those with subtle or no infection (mocks and most decoy-treated mice) (Supplementary Fig. 8a). Corroborating the levels of viral infections observed, differential gene expression (DGE) analysis revealed extensive inflammatory responses in the PBS groups, significantly greater than in mock treatments. At 1, 2, and 4 dpi, 26, 1232, and 1756 genes were upregulated, respectively, and were significantly enriched in Gene Ontology Biological Process (GOBP) terms related to antiviral responses such as type I interferon (IFN) responses and innate immune responses (Fig. 4a,b; Supplementary Fig. 8b–d) [34]. In stark contrast, DGE analysis between B5-D3 prophylaxis and mocks at 1, 2, and 4 dpi showed subtle changes, with only 1, 7, and 32 genes upregulated, respectively, and only moderate enrichment in chemotaxis-related pathways at 4 dpi (Fig. 4c; Supplementary Fig. 8e). The B5-D3-LALA group, however, had 264 genes upregulated at 4 dpi compared to the mocks, suggesting incomplete protection and ongoing viral activity (Fig. 4d; Supplementary Fig. 8f).

To capture the immune activations specifically linked to B5-D3-triggered antiviral efficacy other than infection-induced inflammation, we directly compared the B5-D3 and PBS groups (Fig. 4e-j; Supplementary Fig. 9 and 10). Interestingly, at 1 dpi, the B5-D3 group exhibited enhanced expression of several immune-related genes, including *Lef1* [35], *Fscn1* [36], *Kcne4* [37], *Tcrb*, and *Ccl22* [38, 39], which are associated with early dendritic cell function and T cell activation (Fig. 4e). Gene Set Enrichment Analysis (GSEA) of GOBPs and Kyoto Encyclopedia of Genes and Genomes (KEGG) pathways further supported these findings (Fig. 4f,g). Chemotaxis and pathways related to antigen presentation such as Rap1 signaling pathway [40] and Th1 and Th2 cell differentiation were significantly activated in the B5-D3 group at 1 dpi compared to PBS group (Fig. 4h-j; Supplementary Fig. 9a–c). Moreover, the B5-D3 groups showed enhancement in cilium movement and metabolism of xenobiotics at both 2 and 4 dpi, suggesting active clearance of viral particles due to effective early responses (Supplementary Fig. 10c–f).

Furthermore, we collectively examined the GOBPs that were significantly activated in B5-D3 groups at either 1, 2, or 4 dpi among all treatment groups and time points. Markedly, B5-D3 group showed higher normalized enrichment scores (NES) in chemotaxis-related GOBP pathways than PBS group at 1 dpi (Fig. 4k, purple boxes), while direct comparison between B5-D3 and PBS groups further revealed the broad involvement of multiple types of effector immune cells (Fig. 4l, purple box). These results collectively indicate that early immune activation is a hallmark of B5-D3-mediated protection.

Finally, the lung transcriptomes from mice receiving B5-D3 without viral inoculation showed high similarity to the PBS vehicle controls (Supplementary Fig. 11a). The 10 upregulated genes identified showed poor correlation with the virus-inoculated B5-D3 group (Supplementary Fig. 11b,c), supporting that early immune responses observed in B5-D3 IN prophylaxis groups were primarily triggered by virus neutralization rather than by B5-D3 alone.

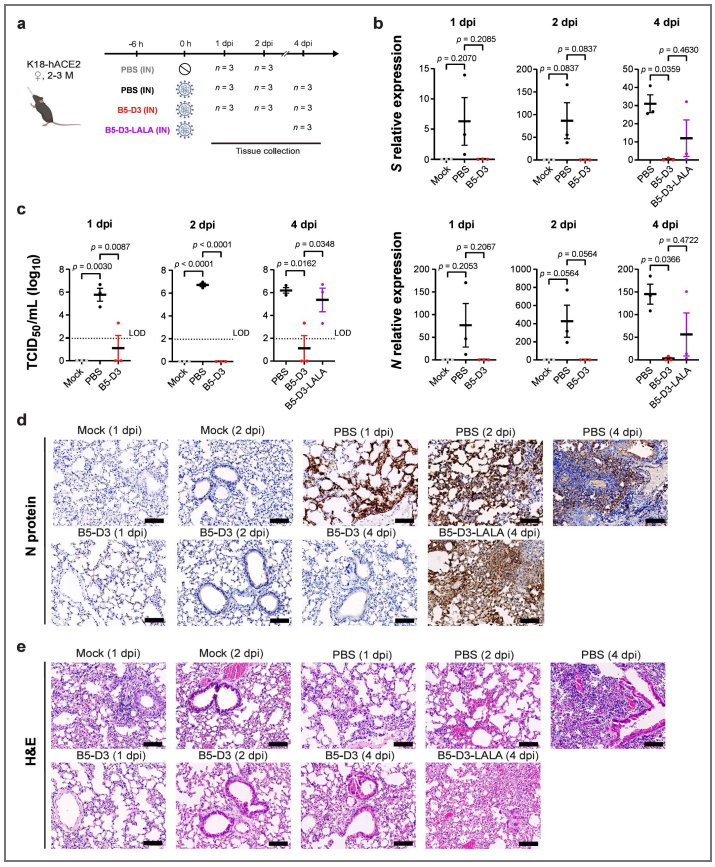

Fig. 3. Efficient viral clearance at early stages through intranasal prophylaxis with B5-D3 against SARS-CoV-2 challenge in K18-hACE2 mice.

a Workflow diagram showing timelines and treatments for different mouse groups. Young female K18-hACE2 mice aged 2 to 3 months received prophylactic administration of PBS (black), B5-D3 (red), or B5-D3-LALA (purple) via the IN route 6 h prior to inoculation with 1×10^4 PFU of Wuhan-Hu-1. Mice inoculated with PBS instead of the virus served as mock controls (grey). Mice from each treatment group were sacrificed for tissue collection at 1, 2, and 4 dpi ($n = 3$ per time point). **b** Quantitative PCR results showing relative amounts of *S* (upper) and *N* (lower) viral RNA in lung tissues collected from different groups at 1, 2, and 4 dpi, normalized to mouse *Gapdh*. **c** The titers of infectious viruses detected in lung homogenates, measured by $TCID_{50}$ assays at 1, 2, and 4 dpi. **d, e** Fixed lung tissues were sectioned and stained; IHC for viral N protein (**d**) and H&E staining for tissue damage (**e**) are shown (scale bar = 100 μm). Data presented as mean ± standard error of the mean (SEM). Statistical significance was determined by Tukey's multiple comparisons test.

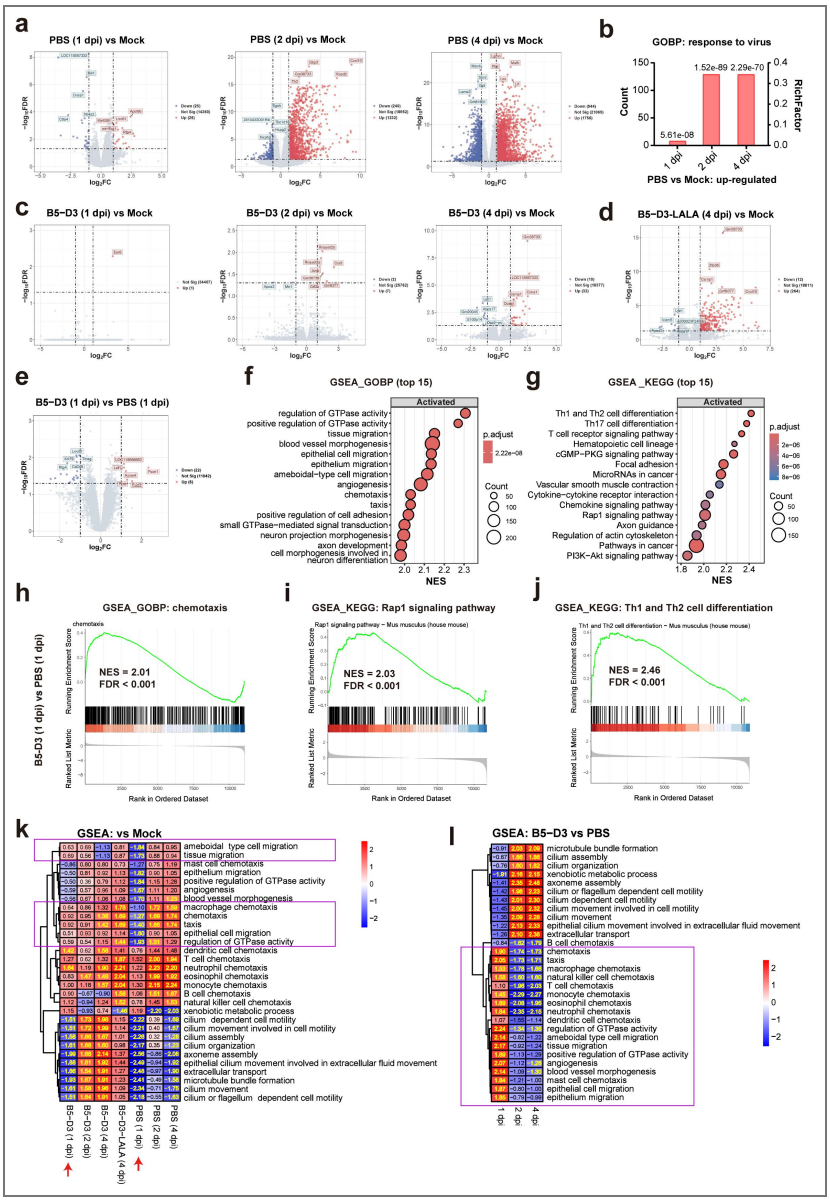

Fig. 4. Transcriptomic analysis of lungs revealed early immune activation in IN B5-D3-prophylaxis mouse group after SARS-CoV-2 challenge.

a–d DGE analysis comparing PBS (**a**), B5-D3 (**c**), and B5-D3-LALA (**d**) against the mock control at specific time points ($n = 3$). Volcano plots illustrate the gene expression changes (**a**, **c**, **d**), while red and blue dots represent significantly upregulated and downregulated genes, respectively, with $|\log_2$ fold change $(\log_2 FC)| \geq 1$ and a false discovery rate (FDR) < 0.05. Bar chart in **b** shows the enrichment of GOBP "response to virus" observed in PBS groups at 1, 2, 4 dpi, in which adjusted *p* values are indicated for individual comparisons. **e–g** Comparison between IN B5-D3 and PBS group at 1 dpi. Volcano plot illustrates the DGE analysis between IN B5-D3 to PBS group at 1 dpi (**e**), with red and blue dots representing significantly upregulated and downregulated genes, respectively, with $|\log_2 FC| \geq 1$ and FDR < 0.05. GSEA shows top 15 significantly activated GOBPs (**f**) and KEGG pathways (**g**) in IN B5-D3 compared to PBS group at 1 dpi. NES, normalized enrichment score; p.adj, adjusted *p* value. **h–j** GSEA plots of chemotaxis (**h**), Rap1 signaling pathway (**i**), and Th1 and Th2 cell differentiation (**j**) in B5-D3 vs PBS comparison at 1 dpi. **k**, **l** Heatmaps show NES of GSEA comparing various treatments to the mock control (**k**) and between B5-D3 to PBS (**l**), focusing on top 10 GOBPs in **f** and Supplementary Fig. 10c, d, respectively, and those related to immune cell chemotaxis. Significant NES values ($p < 0.05$, FDR < 0.25) are highlighted in yellow. Purple boxes indicate GOBPs where B5-D3 (1 dpi) group shows activation but PBS (1 dpi) group shows suppression. Benjamin–Hochberg method was used for FDR adjustment.

Intranasally delivered B5-D3 is enriched in the respiratory tract and targets mainly the airway macrophages

The superior prophylactic antiviral effects of IN over IV administration of B5-D3 as observed in the K18-hACE2 infection experiments (Fig. 2a–e) suggested the importance of mobilizing the local immunity within the respiratory tract. Next, we labeled B5-D3 protein with Alexa Fluor 750 (AF750) and examined its bio-distribution and kinetics after IN administration (Fig. 5a). *In vivo* imaging showed that fluorescence-labeled B5-D3 (B5-D3-AF750) was present in the nasal cavities for at least 24 h after a single IN dose in K18-hACE2 mice (Fig. 5b). *Ex vivo* images further revealed that B5-D3-AF750 distributed in the respiratory tract from nasal cavity to lung within 20 min and remained enriched in lungs by 24 h after administration (Fig. 5c). In contrast, non-respiratory organs showed minimal signals, which were merely detectable in urinary system and liver (Fig. 5d).

To identify the immune cells in the respiratory tract that are actively engaged with IN B5-D3, we performed flow cytometry analysis on bronchoalveolar lavage fluid (BALF) at 6 h after IN administration of B5-D3-AF750 (Fig. 5e). Like normal conditions, over 95% of live BALF cells were $CD45^+$ immune cells, predominantly composed of $CD11c^+Siglec\text{-}F^+$ resident alveolar macrophages (AMs) (> 50%) in both treatment and vehicle groups (Fig. 5f; Supplementary Fig. 12). Notably, the IN administered B5-D3-AF750 was actively retained in the $CD45^+$ cells, with positive rates exceeding 65% in all treated mice (Fig. 5g). Among the $CD45^+B5\text{-}D3^+$ cells, more than 95% were macrophages, composed primarily of $CD11c^+Siglec\text{-}F^+$ AMs (87.2 – 91.7%) and $Siglec\text{-}F^-CD11b^-F4/80^+$ monocyte-derived macrophages (mono-Macs; 6.6 – 9.9%) (Fig. 5h, red arrows). Consistently, these macrophage populations also exhibited the highest B5-D3 positive rates (Fig. 5i,j; Supplementary Fig. 13) and greatest median fluorescent intensities (MFI) (Fig. 5k, red arrows) among all immune cell types in the BALF, indicating the strongest B5-D3-AF750 uptake. Other phagocytic cell types such as the type 2 conventional dendritic cells (cDC2) and monocytes also exhibited considerable AF750 intensities (Fig. 5k, blue arrows; Supplementary Fig. 13b,c), suggesting potential relationships between B5-D3 uptake and phagocytic activities. Confocal microscopy of BALF cells after immunostaining further confirmed that the B5-D3-AF750 were present in the cytoplasm after being retained in AMs (Fig. 5l). These results demonstrate that IN B5-D3 preferentially accumulates in the respiratory tract and is predominantly taken up by airway macrophages, supporting their important role in mediating early immune responses.

sACE2-Fc facilitates phagocytosis of SARS-CoV-2 pseudovirus via mechanisms distinct from ACE2-dependent viral infection

To examine the implication of macrophage involvement in the early immune activation observed in IN B5-D3 treatment groups, we performed cellular analysis using THP-1 cells as an *in vitro* model for phagocytes [41] and examined the sACE2-Fc-dependent phagocytosis of spike-pseudotyped lentiviruses. Indeed, immunostaining of HIV capsid protein p24 confirmed the attachment and entry of pseudoviruses in the THP-1 cells in a B5-D3-dependent manner, with an evidenced signal peak at 6 h post-co-incubation (Supplementary Fig. 14). Interestingly, analysis on the THP-1-derived M0 and M1 macrophages detected even greater p24 signals, indicating stronger phagocytosis activities compared to undifferentiated THP-1 cells (Fig. 6a,b; Supplementary Fig. 15a,b,d,e). This process resembled antibody-dependent cellular phagocytosis (ADCP), which is significant in THP-1-derived M0 and M1 macrophages [42]. Consistently, further examination revealed colocalization of internalized pseudovirus with lysosomal associated membrane protein 1 (LAMP1), indicating trafficking to lysosomes potentially for degradation [43] (Fig. 6c; Supplementary Fig. 15c,f).

We further examined the pseudovirus uptake in Calu-3 cells overexpressing human ACE2 (hACE2-Calu-3; Supplementary Fig. 16) as a model of lung epithelial cells. In contrast to that in macrophages, co-incubation with B5-D3 significantly reduced the pseudovirus entry in hACE2-Calu-3 cells (Fig. 6d–f). Interestingly, while the pseudovirus transduction in hACE2-Calu-3 cells, in the absence of B5-D3, produced robust luciferase signal indicating viral genome release after

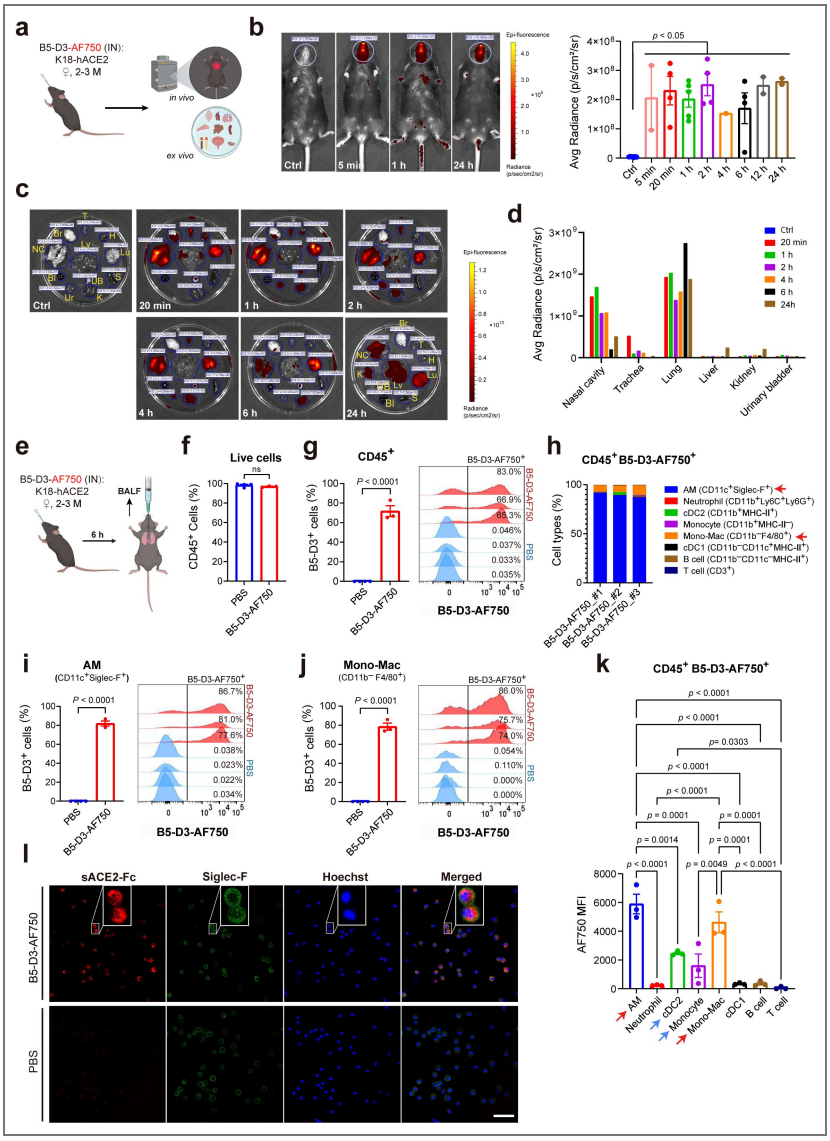

Fig. 5. ***In vivo*** **bio-distribution of B5-D3 after IN administration.**

a Schematic workflow of *in vivo* and *ex vivo* imaging. Female K18-hACE2 mice aged 2 to 3 months received IN administration of fluorescently labeled B5-D3 (B5-D3-AF750) and was visualized at different time points. **b** Representative whole-body images of control and treated mice at 5 min, 1 h, and 24 h after B5-D3-AF750 administration, showing the signal captured by *in vivo* imaging (left). White circles indicate regions of interest (ROIs) for quantification of fluorescence signals in the nasal cavities. Average (Avg) Radiance measured at all time points are shown on the right. **c** *Ex vivo* images of tissues from control and treated mice sacrificed at indicated time points after B5-D3-AF750 administration. Blue circles indicate ROIs for signal quantification. Br, brain; NC, nasal cavity; T, trachea; Lu, lung; H, heart; Lv, liver; S, spleen; K, kidney; UB, urinary bladder; Bl, blood; Ur, urine. **d** Avg Radiance shows the fluorescence signals in excised tissues measured *ex vivo*. **e** Schematic workflow for BALF analysis. Female K18-hACE2 mice aged 2 to 3 months received IN administration of B5-D3-AF750 (n = 3) or PBS (n = 4) and were sacrificed at 6 h later for collection of BALF cells. **f** Percentage of $CD45^+$ cells in live BALF cells. **g** Positive rates (left) and histograms (right) of B5-D3 binding/uptake in $CD45^+$ BALF cells. Histograms show B5-D3-AF750 fluorescence intensities in $CD45^+$ BALF cells from individual mice. **h** Frequency of individual immune cell types in $CD45^+B5\text{-}D3^+$ BALF cells. Red arrows point out AMs and mono-Macs with high abundance. AM, alveolar macrophage; Mono-Mac, monocyte-derived macrophage; cDC1/2, type 1 or 2 conventional dendritic cells. **i, j** Positive rates (left) and histograms (right) of B5-D3 binding/uptake in $CD11c^+Siglec\text{-}F^+$ AMs (**i**) and $CD11b^-F4/80^+$ mono-Macs (**j**). **k** Median fluorescence intensity (MFI) of AF750 indicates B5-D3 binding/uptake in different $CD45^+B5\text{-}D3^+$ populations. **l** Confocal images (scale bar = 50 μm) of BALF cells collected at 6 h and stained for sACE2-Fc (red, anti-Fc, Abcam #ab98596), Siglec-F (green, BD #564514), and nuclei (blue, Hoechst). Magnified views are shown in white rectangles. Data are presented as mean ± SEM, and statistical significance was determined by Tukey's multiple comparisons test or Student's t-test.

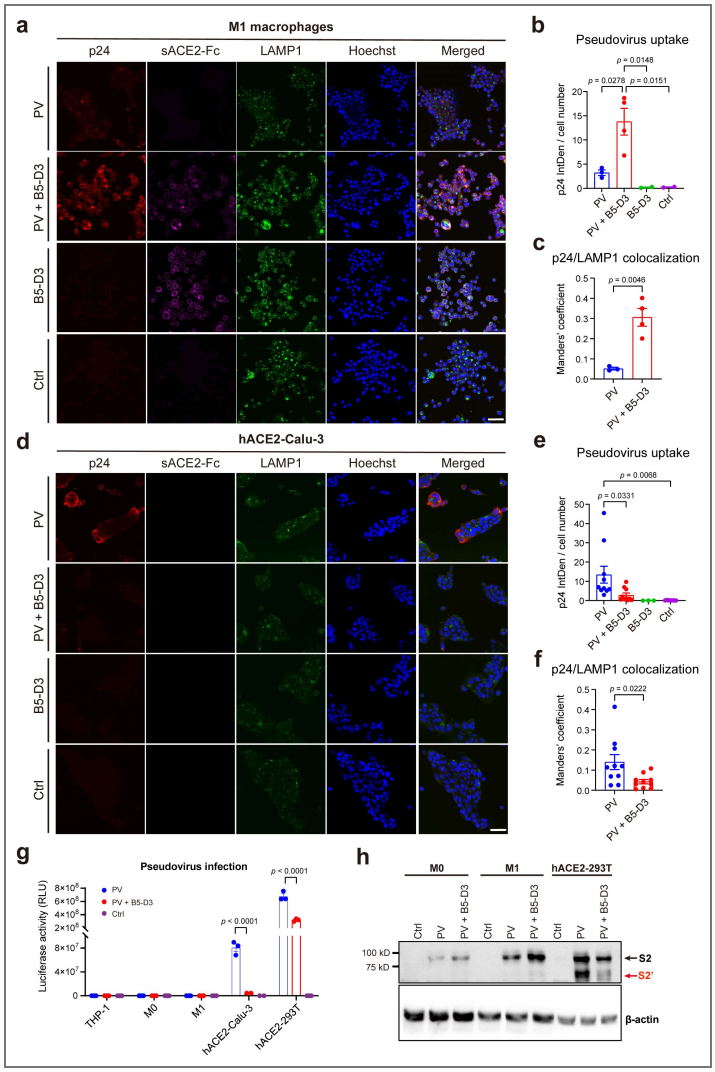

Fig. 6. B5-D3 enhanced phagocytosis and degradation of SARS-CoV-2 pseudovirus in THP-1-derived macrophages.

a Immunostaining of p24 (Invitrogen #PA5-81773), sACE2-Fc, and LAMP1 (Abcam #ab25630) in THP-1-differentiated M0 macrophages showing phagocytosis of SARS-CoV-2 pseudovirus (PV, $p24^{+}$) after 6 h of incubation with or without B5-D3 (scale bar = 50 μm). LAMP1 was stained to identify lysosomes. **b** Quantification of p24 signal intensity as shown in **a**. Intensity Density (IntDen) per cell number indicates the mean p24 signal per cell, calculated using ImageJ. Each dot represents one image. **c** Manders' coefficient indicating the colocalization of p24 and LAMP1 in THP-1 M0 macrophages as shown in **a**. **d** Immunostaining of p24, sACE2-Fc, and LAMP1 in hACE2-Calu-3 cells after 6 h incubation with pseudovirus, with or without B5-D3 (scale bar = 50 μm). **e** Quantification of mean p24 signal intensity as shown in **d**. **f** Manders' coefficient for the colocalization of p24 and LAMP1 in hACE2-Calu-3 cells, as shown in **d**. **g** Quantification of pseudovirus infection in THP-1, M0 macrophages, M1 macrophages, hACE2-Calu-3, and hACE2-293T cells, in the presence or absence of B5-D3. Results shown are luciferase activities measured at 2 days post-transduction. **h** Immunoblot staining of cell lysates to detect SARS-CoV-2 spike cleavage after cell entry. M0 macrophages, M1 macrophages, and hACE2-293T cells were incubated with pseudovirus for 6 h, with or without B5-D3, before protein extraction. Band locations of SARS-CoV-2 spike S2 and S2' fragments are labeled in black and red respectively. Data are presented as mean ± SEM, and statistical significance was determined by Tukey's multiple comparisons test.

cell entry, the evident pseudovirus uptake facilitated by B5-D3 in the THP-1 and derivative macrophages yielded no detectable luciferase activity, which further supported viral degradation within phagolysosomes (Fig. 6g). Corroborating these observations, western blot analysis showed absence of cleaved S2' fragments in the macrophages that had internalized pseudovirus-B5-D3 complexes, supporting that the pseudoviruses did not undergo membrane fusion or cytosolic release as it did in the epithelial cell model [44] (Fig. 6h).

To evaluate the contribution of Fc-mediated effector functions to virus uptake in macrophages, we further compared the efficiencies of B5-D3, B5-D3-LALA, and hIgG1 isotype in mediating pseudovirus uptake by THP-1-derived macrophages (Supplementary Fig. 17). As indicated by p24 staining, functional impairment (LALA mutations) of Fc in B5-D3 significantly reduced the efficiency of virus uptake, emphasizing the importance of intact Fc in B5-D3 function as decoy. Whereas presence of hIgG1 isotype control showed no impact on pseudovirus uptake, supporting that the phagocytosis was largely specific to the pseudovirus-decoy complexes.

To further evaluate the responses triggered by the pseudovirus-B5-D3 complex in macrophages, we performed RNA-seq analysis. The transcriptomic profiling revealed little difference and identified no DEG between the macrophages incubated with both pseudovirus and B5-D3 and those treated with pseudovirus only (Supplementary Fig. 18a). Whereas interestingly, GSEA detected broad activation of pathways related to antiviral response and macrophage activation in the macrophages internalizing pseudovirus and B5-D3 (Supplementary Fig. 18b–i), corresponding to ADCP effect. These findings indicate moderate immune activation triggered by phagocytosis of pseudovirus-decoy complexes, corroborating with the mild immune activation that accelerated antiviral responses in our mice infection experiments.

Collectively, these findings suggest that IN B5-D3 not only blocks viral entry into epithelial cells but also actively redirects SARS-CoV-2 to phagocytic clearance by engaging airway phagocytes via Fc-dependent mechanisms. Moreover, such ADCP-like process contributes to early immune activation and restricts the infection at the respiratory mucosal surface.

Discussion

In this study, we comprehensively evaluated the protective efficacy and mechanistic basis of an optimized representative sACE2-Fc decoy (B5-D3) against SARS-CoV-2 infection. By introducing only two mutations (T92Q and H374N), we generated a minimally engineered sACE2-Fc mutant (B5-D3) that achieved broad-spectrum neutralization with minimal risk of disrupting the RAS. Among various administration routes and dosing schedules examined, we demonstrated that IN prophylaxis of B5-D3 achieved the most robust protection, completely preventing disease in both young and aged K18-hACE2 mice. Transcriptomic analysis of the infected lung samples at early time points revealed distinct IN B5-D3-dependent immune activation at the onset of infection, indicating that B5-D3 acted not only as a receptor decoy but also as an immune engager upon viral infection. Bio-distribution analysis of fluorescence-labeled B5-D3 demonstrated rapid uptake and high accumulation in the respiratory tract, primarily within airway macrophages. Phagocytosis assays further supported that sACE2-Fc decoy mediated a rapid viral clearance in macrophages, while abolishing membrane ACE2-mediated infection in epithelial cells. Together, these findings reveal a dual-function mechanism for sACE2-Fc decoys in redirecting SARS-CoV-2 to phagocytic clearance and rapid immune engagement, supporting their potential as intranasal prophylactics against respiratory viruses.

Previous studies have reported multiple ACE2 mutations with remarkable potential in neutralizing SARS-CoV-2. However, in these studies, combining ACE2 mutations based on *in silico* predictions to both enhance spike binding and eliminate the ACE2 enzymatic activity in a single design resulted in accumulation of mutations such as K31F/N33D/H34S/E35Q/H345L [12] and L79F/M82Y/Q325Y/H374A/H378A [14]. These extensive mutations have been implicated in structural instability [12] and reduced production efficiency [17]. More importantly, the high mutation loads raise risks for immunogenicity, which is a critical issue when considering clinical applications. Corroboratively, Urano *et al.* detected *in vitro* T cell stimulation elicited by the L79F mutation, whereas the T92Q mutation showed much lower immunogenicity and enhanced spike

binding affinity [45]. In our ACE2 decoy design, we incorporated only two mutations (like T92Q and H374N in B5-D3) to enhance neutralization potency while eliminating enzymatic activity, resulting in simplest compound ACE2 mutants. The B5-D3, as a representative, exhibited not only minimal mutation-related risks but also top-level neutralization potencies among all candidate mutants we tested. Hnece, by coupling structural engineering (Fc fusion for avidity improvement) and mutagenesis (potency and safety optimization), we provided simplest decoy design and further consolidated the generalizable framework for decoy design, which is invaluable to combat a novel, highly contagious, and fatal virus in future, before more effective vaccines and drugs are established.

Previous studies have reported that IN prophylaxis with sACE2-Fc mutants or monoclonal antibodies [15, 16, 46] could effectively protect against SARS-CoV-2, in which the Fc-effector functions were indispensable [14]. However, the precise mechanism has not been well depicted, which prevents the further development of these approaches for translation. Here, our study provided evidence for a deeper mechanistic insight, showing that IN sACE2-Fc decoys rapidly engage host immunity in the respiratory tract. Consistently with others' work [14], IN delivery of a Fc-null variant (B5-D3-LALA) resulted in suboptimal protection and higher viral infection compared to B5-D3. Notably, despite the minimal infection observed, B5-D3-treated mice showed robust early immune activation, including induction of antigen presentation and T cell activation within 24 h post-infection (Fig 4). These results support that B5-D3 not only neutralizes virus but also primes innate and adaptive immune responses, counteracting early-stage viral immune evasion.

Furthermore, our bio-distribution data showed that IN-delivered B5-D3 preferentially accumulates in the respiratory tract (Fig. 5a–d). Flow cytometry and confocal imaging confirmed strong binding and uptake of B5-D3 by airway phagocytes, primarily alveolar macrophages and monocyte-derived macrophages (Fig. 5e–l). Notably, phagocytosis assays demonstrated that B5-D3–virus complexes were trafficked to lysosomes for degradation in macrophages. Functional impairment in the B5-D3 structure reduced the uptake of virus by macrophages. These findings support a mechanism in which B5-D3 redirects viral particles away from membrane ACE2-dependent epithelial entry and toward phagocytic clearance (Fig. 7). Importantly, RNA-Seq analysis of macrophages treated with virus-decoy complexes suggests that such ADCP-like process also facilitated early immune activation and initiated downstream antiviral signaling cascades before the virus reaches epithelial targets (Fig. 7b). Hence, the IN prophylaxis offers a unique advantage by enabling localized immune priming and efficient viral clearance at the frontline of infection. The IN-administered antibody drugs can share similar mechanism and confer effective protection against primary infection of SARS-CoV-2 or other respiratory viruses. However, antibody drugs can be easily escaped when new viral variants emerge, which is specifically common among rapidly spreading respiratory RNA viruses [47]. In contrast, the decoy strategy is intrinsically resistant to "antigenic escape" of the mutating virus, which is further supported by the trend observed in viral evolution that later-emerging SARS-CoV-2 variants exhibit a higher affinity for the ACE2 receptor, enhancing their infectivity and transmissibility [16].

In a post-infection context, respiratory viruses would have propagated extensively at the primary infection site when symptoms arise, which makes IN neutralization relatively ineffective to clear the high viral burden and the resultant systematic inflammation [48]. Therefore, the therapeutic activity of either local or systemic neutralization at post-infection stage is bound to be restricted, which is intrinsically inherited in all decoy/antibody therapies against respiratory viral infections. Yet, transfusion of convalescent plasma or infusion of neutralizing mAbs in clinical practice have been shown to reduce the mortality in COVID-19 [49, 50], and IV administration of B5-D3 as therapy was also shown effective in improving the viral burden and survival in our aged mouse experiment (Fig. 2a–e). Therefore, the therapeutic value of our decoy strategy does exist when a "systematic" route of administration (*e.g.*, IV infusion) is chosen, and improvement in disease severity should thus be expected.

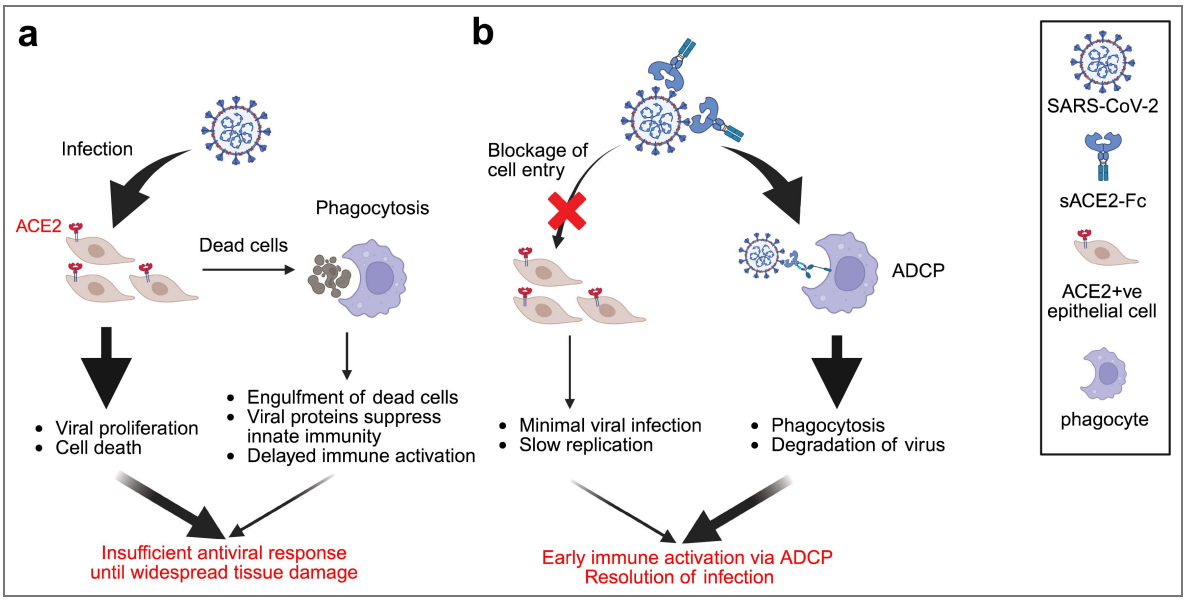

Fig. 7. Proposed mechanisms of action of IN sACE2-Fc decoy in preventing SARS-CoV-2 infection.

a, b Schematics illustrating the actions and outcomes of SARS-CoV-2 infection, in the absence (**a**) and presence (**b**) of IN delivered sACE2-Fc decoys. The figure was created in *BioRender.com*.

Our study has several limitations. First, we didn't examine the potential of IgM-based sACE2 decamers, which showed higher avidity to spikes and greater potency for viral neutralization in previous studies [46, 51, 52]. It is promising that our B5-D3 design would benefit from switching to the IgM isotype, whereas the distinct biological features imposed by IgM Fc, including short serum half-life and restricted tissue penetration [53], may complicate the analysis design and diverge our study focus. Moreover, although no sign of B5-D3-specific immune responses was observed in our AAV-injected mice, its immunogenicity and potential risk for antibody-dependent enhancement (ADE) should be thoroughly evaluated to further develop the decoy strategy for human use. Furthermore, despite that K18-hACE2 mice are broadly used and demonstrate the best susceptibility to SARS-CoV-2 infection among established hACE2-transgeic mouse models [54], hACE2 expression in these mice shows a distinct pattern that may not reflect human physiology [31, 55]. Further study on hACE2 decoy using animals with physiological level of hACE2 expression and humanized immune system that can support stable engraftment of myeloid lineages would be warranted.

In conclusion, we present a rationally designed sACE2-Fc decoy with minimal mutagenesis (B5-D3) and provide compelling evidence and insights into the immune mechanism supporting its potent prophylactic efficacy. Intranasal prophylactic administration of B5-D3 not only neutralizes SARS-CoV-2 but also redirects the virus toward phagocytic clearance, enabling early immune engagement and complete protection. These findings provide a mechanistic basis for decoy-based antiviral strategies and offer a promising approach to combat current and future airborne viral threats. Further studies may aim to develop approaches to enhance the rapid local immune engagement to restrict early viral propagation. Additionally, regimen refinements are needed to enhance stability and functionality of decoy-based treatments before their clinical translation and extension to a broader range of respiratory pathogens.

Materials and methods

Plasmid construction

The coding sequence of human ACE2 was cloned into the pGEM-T easy vector (Promega) and underwent site-directed mutagenesis [10–12, 17]. The sACE2 and human IgG1 hinge-Fc regions (aa 216-447) were assembled via overlapping PCR. These constructs, along with 6xHis-tagged versions, were inserted into the HDM-SARS2-Spike-delta21 vector (Addgene #155130) to generate HDM-CMV-sACE2(-Fc)-his plasmids. L234A/L235A (LALA) in hIgG1 were introduced to generate HDM-CMV-sACE2-Fc-LALA-his plasmids. Various sACE2-Fc fragments were then subcloned into pAAV-nEFCas9 vector (Addgene #87115) to generate AAV-nEF-sACE2-Fc plasmids. SARS-CoV-2 spike variants with or without an HA tag fused to the C-terminal were synthesized and inserted into the HDM vector [56].

Protein structure visualization

The crystal structure of SARS-CoV-2 spike receptor-binding domain bound with ACE2 (6M0J)was downloaded from the Protein Data Bank (PDB, *https://www.rcsb.org/structure/6m0j*) [57]. Color-labeling of individual amino acids was performed on the PDB website. For structural overlapping analysis of WT sACE2 and B5-D3 (aa 18-740), protein structures were predicted using online AlphaFold 3 server (*https://alphafoldserver.com/*) [22]. PyMOL was utilized for root mean square deviation (RMSD) calculations and structural visualization.

Cell culture

293T, Vero E6, Calu-3, and THP-1 cells were obtained from the American Type Culture Collection and incubated at 37 °C with 5% CO_2. Specifically, 293T, Vero E6, and Calu-3 cells were maintained in Dulbecco's Modified Eagle Medium (DMEM, Gibco) supplemented with 10% fetal bovine serum (FBS, Gibco) and 1% Penicillin-Streptomycin (PS, Gibco). THP-1 cells were cultured in Roswell Park Memorial Institute 1640 medium (RPMI, Gibco) with similar supplements. THP-1 cells were differentiated into M0 macrophages using 50 nM phorbol 12-myristate 13-acetate (PMA) for 48 h,

followed by a 24 h rest. For M1 macrophage differentiation, post-PMA treatment cells were stimulated with 10 ng/mL lipopolysaccharide and 20 ng/mL interferon (IFN)-γ for 24 h. Expi293 cells (Gibco) were cultured following the manufacturer's instructions.

Immunofluorescence staining of hACE2-293T and hACE2-Calu-3

Cells were fixed, permeabilized, and blocked with 10% Normal Goat Serum (Invitrogen). ACE2 was stained with a primary antibody (Abcam #ab15348) followed by an Alexa Fluor 594-conjugated secondary antibody (Invitrogen #A-21442). Cells were counterstained with Hoechst 33342 (Thermo Scientific) and examined under Nikon Ti2-E Inverted Fluorescence Microscope.

Lentivirus packaging and transduction

293T cells were seeded at 80% confluence and transfected with psPAX2 (Addgene #12260), pMD2.G (Addgene #12259), and transfer plasmid pWPI-IRES-Puro-Ak-ACE2-TMPRSS2 (Addgene #154987) using polyethylenimine (PEI). Lentivirus-containing medium was harvested 72 h post-transfection, filtered through a 0.45 μM filter, concentrated, and stored at −80°C. For transduction, 293T or Calu-3 cells were exposed to the concentrated lentivirus with 8 μg/mL polybrene for 24 h to obtain human ACE2-overexpressing cell lines (hACE2-293T and hACE2-Calu-3 respectively).

Pseudovirus packaging, titration, and infection

Pseudoviruses were packaged in 293T cells using pCDH-EF1a-eFFly-eGFP (Addgene #104834) and spike-encoding plasmids, following a similar protocol to that of lentivirus. Post-packaging, pseudoviral particles were titrated using the Lenti-X qRT-PCR Titration Kit (Takara #631235) and used to infect target cells in the presence of 8 μg/mL polybrene. Infectivity was assessed via a luciferase assay (Promega #E1501).

Protein production and purification

293T and Expi293 cells were transfected with HDM-CMV-sACE2(-Fc)(-LALA)-his plasmids using PEI and ExpiFectamine 293 Transfection Kit (Gibco) respectively. Culture supernatants were collected after 72 h and 5 days post-transfection respectively. The 293T supernatant was assessed for ACE2 and IgG1 levels using enzyme-linked immunosorbent assay (ELISA) kits (Abcam #ab235649; Invitrogen #BMS2092), and ACE2 activity was measured with a fluorometric assay (Abcam # ab273297). The Expi293 supernatant underwent Ni-NTA Agarose purification, followed by elution and buffer exchange to phosphate-buffered saline (PBS, pH 7.4). Protein concentration and integrity were verified using the Bradford method, ELISA, and sodium dodecyl sulfate-polyacrylamide gel electrophoresis (SDS-PAGE).

In vitro pseudovirus neutralization assay

Conditioned media containing sACE2, sACE2-Fc or sACE2-Fc-LALA proteins were diluted serially, mixed with pseudovirus (4×10^9 copies), and incubated at room temperature for 30 minutes [19]. The mixture was added to hACE2-293T cells in 96-well plates with duplicates with 8 μg/mL polybrene. Transduction efficiency was assessed 48 h later via green fluorescent protein (GFP) imaging and/or luciferase assays.

Reporter-based *in vitro* ADCC and ADCP assays

The *in vitro* antibody-dependent cell-mediated cytotoxicity (ADCC) and antibody-dependent cellular phagocytosis (ADCP) activities of B5-D3(-LALA) were measured using Jurkat-Lucia NFAT-CD16 and Jurkat-Lucia NFAT-CD32 cells (InvivoGen) respectively according to the manufacturer's instructions. 293T cells transfected with pBOB-CAG-SARS-CoV-2-Spike-HA (Addgene #141347) acted as target cells. Target cells were co-incubated with reporter cells and serially diluted B5-D3(-LALA) at 37°C for 1 h. Luciferase expression indicating CD16 and CD32 signaling was measured using QUANTI-Luc (InvivoGen).

ADCP of pseudovirus in THP-1 and THP-1-derived macrophages

SARS-CoV-2 pseudovirus (Wuhan-Hu-1, 8×10^8 copies in 10 µL) was mixed with 50 µL of B5-D3 or control proteins (20 µg/mL) and added to THP-1, M0, or M1 cells cultured in a µSlide 18 Well iBITreat chamber slide. Here THP-1 cells were attached on the collagen-coated iBITreat chamber slide. After 1, 3, 6, or 18 hours of incubation for phagocytosis, cells were fixed with ice-cold methanol for 10 minutes, blocked with 10% normal goat serum for 1 hour at room temperature, and immunostained sequentially for human IgG-Fc (Abcam #ab98596), HIV-1 p24 (Invitrogen #PA5-81773), and lysosomal associated membrane protein 1 (LAMP1) (Abcam #ab25630). Secondary antibodies were applied (Invitrogen #A-21200 and #A-31573), and nuclei were stained with Hoechst. Imaging was conducted using a Leica SP8 confocal microscope. p24 immunofluorescence intensity and colocalization with LAMP1 (Manders' coefficient) were analyzed using ImageJ and the JACoP plugin.

For RNA extraction, M0 cells were washed once with PBS and added with TRIzol (Invitrogen) after 6 h incubation with pseudovirus with/without B5-D3 (n = 3 in triplicate wells).

Western blot for spike cleavage detection

SARS-CoV-2 spike-HA tagged pseudovirus (4×10^9 copies) was incubated with M0/M1 macrophages or hACE2-293T cells for 6 h, with or without sACE2-Fc proteins. After incubation, cell lysates were processed through SDS-PAGE and transferred to polyvinylidene difluoride membranes. The membranes were blocked, incubated overnight with anti-HA (Merck Millipore #05-904) and anti-β-actin (Santa Cruz #sc-47778) primary antibodies, then with horseradish peroxidase (HRP)-conjugated secondary antibodies (Cell Signaling Technology #7076). Signals were detected using the Amersham ECL select kit on a Bio-Rad ChemiDoc MP system.

AAV vector packaging and purification

As described previously [58], AAV vectors were produced in 293T cells transfected with AAV-nEF-sACE2-Fc, pAdDeltaF6 (Addgene #112867), and pAAV2/8 (Addgene #112864) plasmids using PEI. AAV particles were harvested from supernatants with Polyethylene Glycol (PEG) 8000 and from cell lysates via freeze-thaw cycles and benzonase digestion, then purified using Iodixanol density gradient ultracentrifugation. AAV particles were concentrated and measured using a qPCR AAV Titer Kit (Applied Biological Materials #G931).

SARS-CoV-2 virus

Experiments with live SARS-CoV-2 were performed at the BSL-3 core facility (LKS Faculty of Medicine, HKU). The BetaCoV/Hong Kong/VM20001061/2020 virus, here regarded as the wild type strain of SARS-CoV-2 (Wuhan-Hu-1), was isolated from the nasopharyngeal aspirate and throat swab of a confirmed patient with COVID-19 in Hong Kong (GISAID identifier EPI_ISL_412028). The SARS-CoV-2 variants were isolated from clinical specimens in Hong Kong. Stock viruses were prepared with Vero E6 cells cultured in infection medium (DMEM supplemented with 2% FBS and 1% PS).

Median tissue culture infectious dose ($TCID_{50}$) assay

Vero E6 cells pre-seeded in 96-well plates were infected with serially diluted virus stocks or mouse lung homogenates in infection medium. After 72 h incubation, cytopathic effects (CPEs) were observed under a microscope to calculate titers using the Reed–Muench method.

Plaque-reduction neutralization test (PRNT) assay

Casirivimab (#C100P) and hIgG1 isotype (clone 4F17, #PA007125) were purchased from Syd Labs, USA) and used as controls. Purified B5-D3 and control proteins were serially diluted and incubated with 50 PFU of SARS-CoV-2 (Wuhan-Hu-1, Delta, Omicron BA.5, BQ.1.22, and XBB.1.5) for 1 h at room temperature, followed by addition to Vero E6 cells seeded in 6-well plates. After incubation,

cells were overlaid with agarose, fixed with formalin, and stained with crystal violet. Plaque counts were used to calculate percentage neutralization and half maximal inhibitory concentration (IC_{50}) values. The experiments were carried out in duplicates.

Animal experiments

The K18-hACE2 mice (B6.Cg-Tg(K18-ACE2)2Prlmn/J) [31] were purchased from the Jackson Laboratory (Bar Harbor, ME, USA). Experiments on AAV or protein-only administration in mice were carried out in the Animal Holding Core of the School of Biomedical Sciences, CUHK. Experiments involving SARS-CoV-2 infection in K18-hACE2 mice were conducted within the confines of the Biosafety Level 3 (BSL-3) core facility located at the Li Ka Shing Faculty of Medicine, HKU. Experiments were conducted according to ethical practices to minimize animal distress.

AAV-mediated sACE2-Fc overexpression in mice

Male K18-hACE2 mice [31] at the age of 2 months were injected intravenously with 1×10^{11} GC of AAV-nEF-sACE2-Fc. Blood samples were collected periodically for analysis. Following euthanasia, tissues were harvested for further DNA and histological analysis. sACE2-Fc concentrations in sera and RAS metabolites were quantified using specific ELISA kits for Human IgG1, Mouse Renin 1 (Invitrogen #EMREN1), Angiotensin II (LifeSpan BioSciences #LS-F523), and Angiotensin 1-7 (LifeSpan BioSciences #LS-F40645).

SARS-CoV-2 infection in mice

Female K18-hACE2 mice, aged 10-12 months or 2-3 months, were intranasally inoculated with $1{\times}10^4$ plaque-forming unit (PFU) of SARS-CoV-2 Wuhan-Hu-1. Treatment with B5-D3 protein was administered intranasally at 2.5 mg/kg or intravenously at 15 mg/kg, at various time points relative to the viral challenge (6 h before, 24 h before, or 24 h after). Vehicle control groups received PBS 6 h before viral challenge. Survival and weight were monitored daily for 14 days. For the older mice, lung samples were collected from one mouse from each group at 4 days post-infection (dpi) for analysis; younger mice had plasma collected for neutralizing antibody analysis at 14 dpi. Another batch of young mice also received B5-D3(-LALA) protein pre-inoculation, with lungs analyzed post-inoculation for RNA, viral load, and histopathology. A control group of non-infected mice was used to assess baseline effects of B5-D3 on lung tissue.

Neutralization assay for antibody titration

Vero E6 cells were pre-seeded on 96-well plates 24 h before infection. On the day of infection, the growth medium of the cells was changed to infection medium. The plasma samples were serially 2-fold diluted with infection medium from a starting dilution of 1:10. The plasma was then pre-incubated with 100 $TCID_{50}$ of SARS-CoV-2 for 1 h at room temperature before being inoculated to the seeded Vero E6 cells in quadruplicates. At 72 h after inoculation, CPEs of the cells were observed with optical microscopy. Neutralizing antibody titers against SARS-CoV-2 were expressed as the reciprocal of the highest dilution of plasma showing no CPEs in all 4 wells. Uninfected cell monolayers were used as toxicity control.

Histology

Mouse tissues were fixed in 10% formalin, embedded in paraffin, and sectioned at 5 μm. Sections of different organs were deparaffinized and underwent hematoxylin and eosin (H&E) staining. For immunohistochemistry (IHC) staining, lung sections underwent antigen retrieval, endogenous peroxidase blocking, and were incubated with primary antibodies against the SARS-CoV/SARS-CoV-2 nucleocapsid protein (Sino Biological #40143-T62) overnight. After washing, sections were stained with the anti-rabbit VECTASTAIN Elite ABC-HRP Kit (Vector Laboratories), developed with 3,3'-Diaminobenzidine (Sigma #D4293), and counterstained with Mayer's hematoxylin. Stained sections were scanned using Zeiss Axioscan 7 and analyzed using ZEN (blue edition). For measurement of alveolar septal thickness, 10 fields from each lung H&E section and 10 septa from each field were chosen for measurement using ImageJ.

Quantitative PCR

Quantitative PCR (qPCR) was used to analyze liver genomic DNA and lung RNA from mice. DNA was extracted and qPCR was performed with the TB Green Premix Ex Taq II kit (Takara), normalized to mouse *Gapdh* using the 2^-ΔCt method. RNA was extracted using TRIzol, reverse-transcribed (Applied Biosystems #4368813), subjected to qPCR using the same kit and normalized to mouse *Gapdh* levels. Specific primers are listed in Supplementary Table 2.

RNA-Seq and data analysis

Total RNA was extracted from mouse lung tissues or THP-1-derived M0 macrophages using TRIzol and processed into transcriptome libraries with the TruSeq RNA Library Prep Kit (illumina). Sequencing was performed on the NovaSeq 6000 or NovaSeq X Plus sequencers (illumina) using a 150-base pair paired-end configuration. Sequencing data were processed with fastp for quality control [59], then aligned to both the mouse (Ensembl GRCm39) and SARS-CoV-2 (NCBI NC_045512v2) genomes using STAR [60] or to the human genome (Ensembl GRCh38) using HISAT2 [61]. Pearson correlation and groupwise comparisons were conducted in R: gene expression was quantified and analyzed for differential expression using DESeq2 [62]; up/downregulated gene enrichment and Gene Set Enrichment Analysis (GSEA) [63] was performed using the clusterProfiler package [64].

Tracking B5-D3 bio-distribution in mice

B5-D3 were conjugated with Alexa Fluor 750 dye (B5-D3-AF750) as described [46]. In brief, 2 mg/mL solution of B5-D3 protein in 0.15 M $NaHCO_3$ was reacted with Alexa Fluor 750 succinimidyl ester (Thermo Fisher Scientific) at room temperature for 1 h. Unreacted dye was removed by dialysis in PBS. All procedures were performed under dimmed light. Female K18-hACE2 mice, aged 2-3 month, were administered intranasally with B5-D3-AF750 (2.5 mg/kg). The mice were imaged at predetermined time points after administration (fluorescence ex = 745 nm, em = 800 nm, auto-exposure setting) using an IVIS Spectrum CT Imager (Perkin Elmer). At the time of euthanasia, 50 µL of urine and blood, the brain, nasal cavity, trachea, lung, heart, liver, spleen, kidney, and urinary bladder samples were excised and imaged. Regions of interest (ROIs) were drawn, and average radiance (p/s/cm²/sr) was measured. All images were processed using Living Image software (Perkin Elmer) and the same fluorescence threshold was applied for group comparison.

Flow cytometry analysis and confocal microscopic imaging of BALF cells

Mice were sacrificed via anesthetics overdose. Bronchoalveolar lavage was performed by intratracheally rinsing the lungs with 1 mL of ice-cold Hanks' Balanced Salt Solution (HBSS, Gibco) containing 100 µM ethylenediaminetetraacetic acid for four repeats. Bronchoalveolar lavage fluid (BALF) was then centrifuged and treated with ammonium-chloride-potassium red blood cell lysing buffer. For multicolor flow cytometry, cell pellets were washed with PBS and stained with the Fixable Viability Stain 440UV dye (BD #566332). Next, the cells were blocked with CD16/CD32 monoclonal antibody (Invitrogen #14-0161-85) and stained with antibodies targeting the following molecules: CD45 (BD #568336), Siglec-F (BD #564514), CD11b (BD #612800), CD11c (BD #751265), Ly6G (BD #563005), I-A/I-E major histocompatibility complex class II (MHC-II) (BD #750171), F4/80 (BD #570288), Ly6C (BD #755198), and CD3 (BD #555275). Stained BALF cells were analyzed using the BD FACSymphony A5.2 SORP Flow Cell Analyzer, and the results were analyzed using FlowJo v10.10.

For microscopic inspections, BALF cells were collected from mice, seeded in poly-d-lysine-coated chamber slides and stained with antibodies targeting Siglec-F (BD #564514) and human IgG-Fc (Abcam #ab98596). Secondary antibody (Invitrogen #A-11006) was applied. Stained BALF cells were then counterstained with Hoechst and examined by confocal microscopy (Leica TCS SP8).

Statistical Analysis

Assays including *in vitro* neutralization, PRNT, ADCC, and ADCP were conducted in technical duplicates. Results were analyzed in GraphPad Prism version 9 using nonlinear regression to calculate IC_{50} or half maximal effective concentration (EC_{50}) values. Transcriptomic analyses were performed using R, with details provided in figure captions. All other statistical analyses utilized GraphPad Prism version 9 with a significance threshold set at p value (p) < 0.05.

Supplementary Information

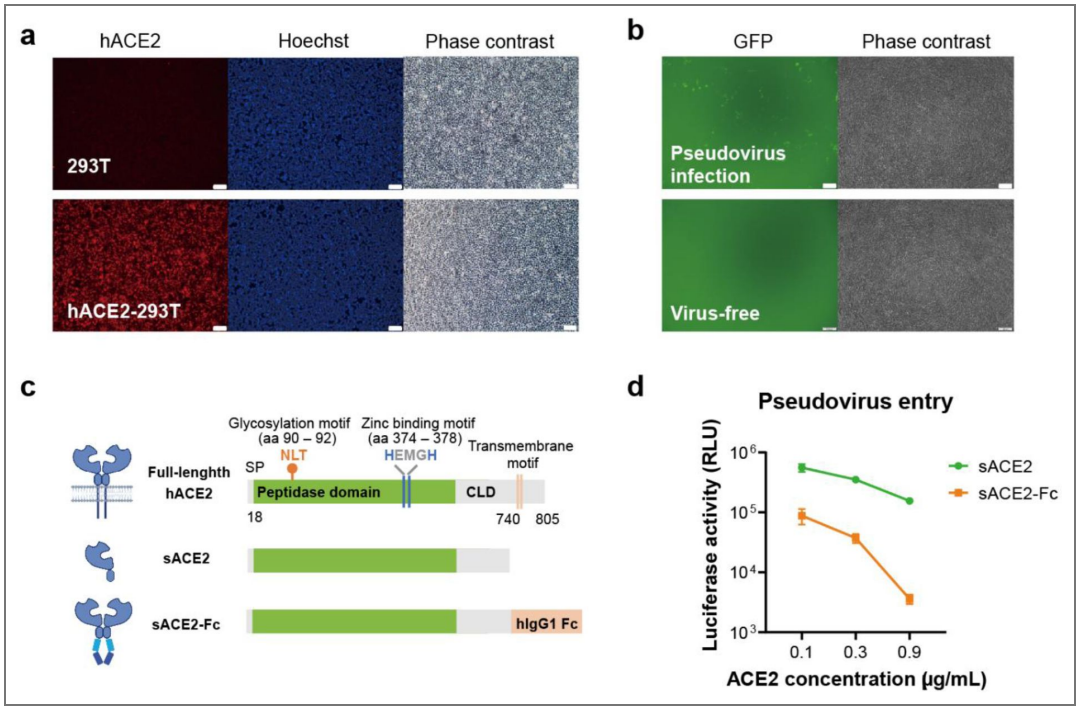

Supplementary Fig. 1. Establishment of the pseudoviral infection platform and generation of sACE2 decoys. **a** Microscopic images show the expression of full length human ACE2 (hACE2) in stable hACE2-293T cells established by lentiviral transduction (Scale bar = 100 μm). Immunostaining was performed using antibody specific to hACE2 (Abcam # ab15348). **b** Representative fluorescence and phase contrast images showing GFP expression in hACE2-293T cells with and without infection by pseudovirus carrying the Wuhan-Hu-1 spike protein (Scale bar = 100 μm). **c** Schematic diagrams of hACE2 (top), sACE2 (middle), and sACE2-Fc (bottom) molecules indicating important amino acid positions (90-92 and 374-378) for glycosylation and zinc binding. aa, amino acid. **d** Line chart comparing the neutralization efficiencies of sACE2 (green) and sACE2-Fc (orange) against Wuhan-Hu-1 pseudovirus expressing luciferase, measured in relative luminescence units (RLU). Data are presented as mean ± SD from duplicate experiments.

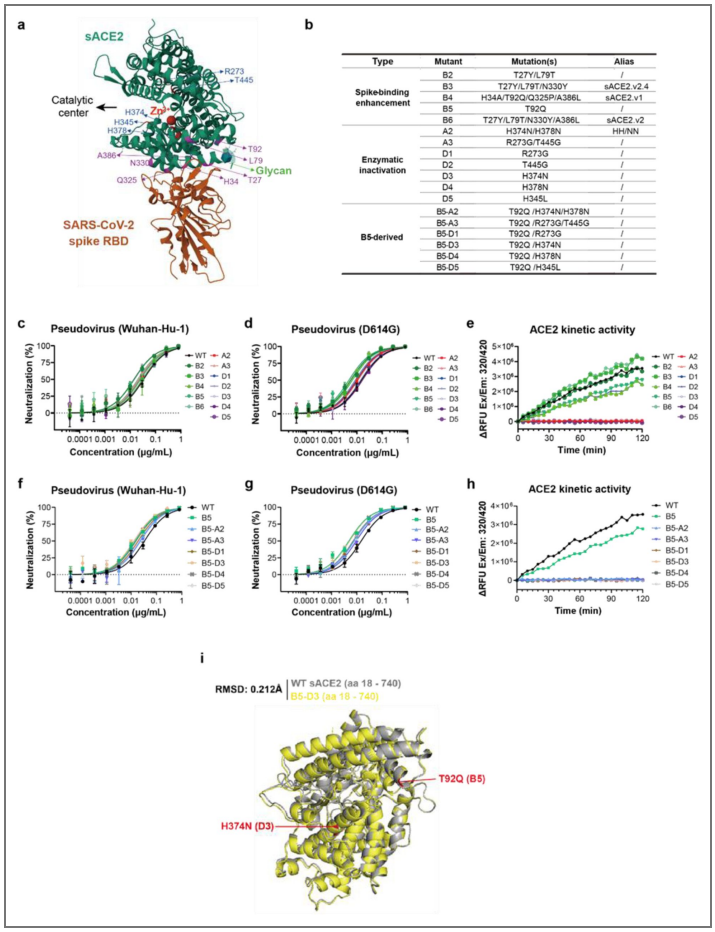

Type	Mutant	Mutation(s)	Alias
Spike-binding enhancement	B2	T27Y/L79T	/
	B3	T27Y/L79T/N330Y	sACE2 v2.4
	B4	H34A/T92Q/Q325P/A386L	sACE2 v1
	B5	T92Q	/
	B6	T27Y/L79T/N330Y/A386L	sACE2 v2
Enzymatic inactivation	A2	H374N/H378N	HH/NN
	A3	R273G/T445G	/
	D1	R273G	/
	D2	T445G	/
	D3	H374N	/
	D4	H378N	/
	D5	H345L	/
B5-derived	B5-A2	T92Q /H374N/H378N	/
	B5-A3	T92Q /R273G/T445G	/
	B5-D1	T92Q /R273G	/
	B5-D3	T92Q /H374N	/
	B5-D4	T92Q /H378N	/
	B5-D5	T92Q /H345L	/

Supplementary Fig. 2. Engineering and characterization of enhanced sACE2 decoys.

a 3D structural model of ACE2 (green) complexed with the SARS-CoV-2 spike receptor-binding domain (RBD, brown), highlighting mutations for spike-binding enhancement (magenta) and enzymatic inactivation (blue). Structures were adapted from Protein Data Bank (PDB ID: 6M0J). **b** List of mutations in sACE2 sequences tested for enhanced binding or enzymatic inactivation. **c**, **d** Neutralization assay results for WT sACE2-Fc and mutants (B2 to B6, A2, A3, and D1 to D5) against Wuhan-Hu-1 (**c**) and D614G (**d**) pseudoviruses. **e** Kinetic curves showing the ACE2 enzymatic activities of WT sACE2-Fc and B2 to B6, A2, A3, D1 to D5 mutants. **f**, **g** Neutralization results for WT sACE2-Fc and mutants (B5, B5-A2, B5-A3, B5-D1, B5-D3, B5-D4 and B5-D5) against Wuhan-Hu-1 (**f**) and D614G (**g**) pseudoviruses. **h** Kinetic curves showing the ACE2 enzymatic activities of WT sACE2-Fc and B5, B5-A2, B5-A3, B5-D1, B5-D3, B5-D4 and B5-D5 mutants. **i** Conformational comparison between WT and B5-D3 sACE2. The 3D structures of WT and B5-D3 sACE2 (aa 18–740) were predicted using AlphaFold 3 and superimposed for direct comparison. The WT sACE2 structure is coloured in grey, while the B5-D3 variant is highlighted in yellow. Mutations in the B5-D3 structure are specifically marked in red. Data are presented as mean ± SD from duplicate experiments.

Supplementary Fig. 3. Broad-spectrum neutralization against pseudoviruses of SARS-CoV-2 VOC/VOI strains by sACE2-Fc candidate mutants.

Graphical representation of dose-response curves in neutralization assays against pseudoviruses bearing spikes from various SARS-CoV-2 VOCs and VOIs. Data are presented as mean ± SD from duplicate experiments.

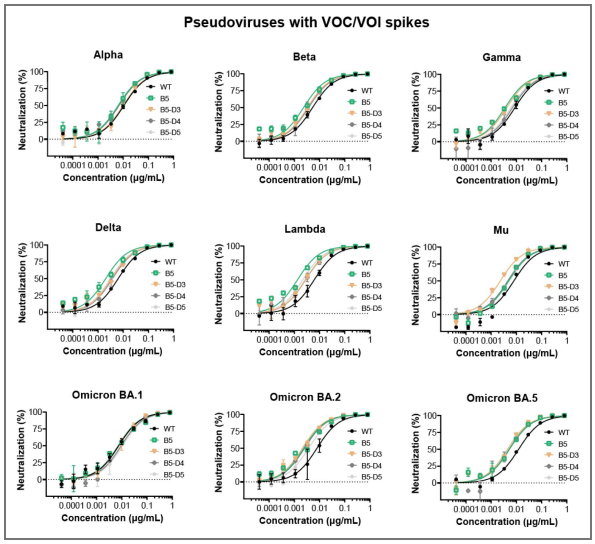

Supplementary Fig. 4. AAV-delivered prolonged overexpression of WT sACE2-Fc and candidate mutants in K18-hACE2 mice.

a Schematic of AAV administration. Male K18-hACE2 mice aged 2 months received tail vein injections of either PBS (black; *n* = 7) or AAV carrying WT sACE2-Fc (blue), B5-D3 (orange), B5-D4 (dark grey), or B5-D5 (light grey) (*n* = 4 each) at a dose of 1 × 10^{11} GC. Mice were observed for up to 15 weeks and then sacrificed for tissue analysis. wpi, weeks post-injection; M, month. **b** Serum concentrations of sACE2-Fc were quantified via ELISA using antibodies specific to hIgG1. **c** Quantification of AAV genomes in the mouse livers at the observation endpoint. Results shown are from qPCR of genome DNA normalized to mouse *Gapdh.* **d–f** Concentrations of renin (**d**), Ang II (**e**), and Ang (1-7) (**f**) in sera at 2 wpi, measured via metabolite-specific ELISA. ns, not significant with *p* value (*p*) ≥ 0.05. **g** Representative H&E staining of heart, lung, liver, kidney, spleen, ileum, and colon tissues from mice in the PBS, WT sACE2-Fc, and B5-D3 treatment groups (scale bar = 50 μm). Data are presented as mean ± SEM. Statistical analyses were performed using one-way analysis of variance (ANOVA) and Tukey's multiple comparisons test following ANOVA.

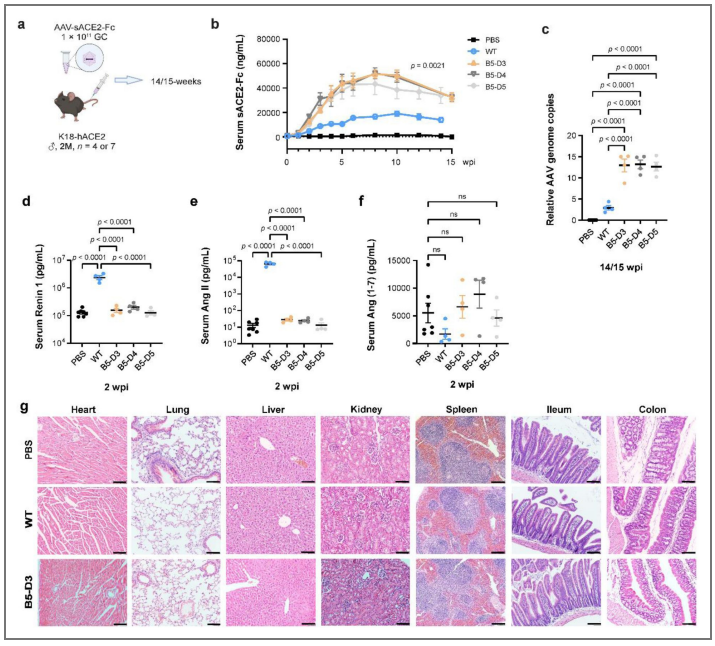

Supplementary Fig. 5. Comparison between B5-D3 and B5-D3-LALA in *in vitro* neutralization against the SARS-CoV2 pseudovirus and Fc-mediated effector functions.

a Neutralization capability of B5-D3-LALA was compared to B5-D3 using an *in vitro* pseudovirus neutralization assay. IC_{50} values are indicated for each version. **b**, **c** Fc-mediated effector functions of B5-D3 and B5-D3-LALA were assessed using luciferase-based reporter cell lines. Dose-response curves and half maximal effective concentration (EC_{50}) values for antibody-dependent cellular cytotoxicity (ADCC) (**b**) and antibody-dependent cellular phagocytosis (ADCP) (**c**) are displayed. Data are presented as mean ± SD from duplicate experiments.

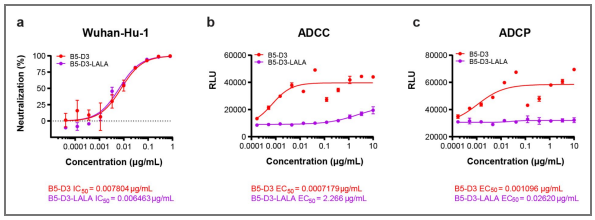

Supplementary Fig. 6. Entire sections for histological examination at 1 dpi.

Fixed lung tissues were sectioned and stained for histological examination. IHC staining for viral N protein (left panels, SinoBiological # 40143-T62) and H&E staining for tissue damage (right panels) are displayed. Black arrows in H&E photos indicate areas of alveolar thickening. Scale bar = 500 μm.

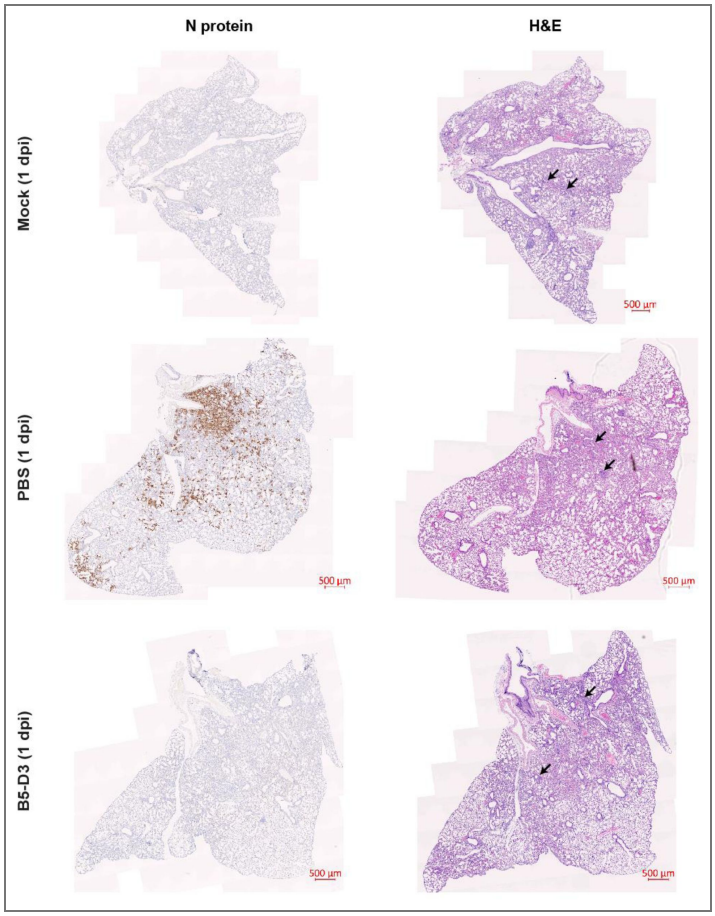

Supplementary Fig. 7. Thickening of alveolar septum in K18-hACE2 mice after SARS-CoV-2 challenge.

Lung septum thickness of K18-hACE2 mice in Fig. 3 was measured from H&E staining. Data are presented as mean ± SEM, and statistical significance was determined by Tukey's multiple comparisons test.

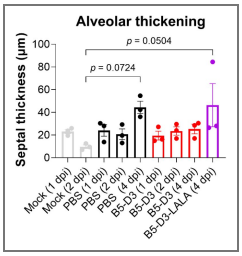

Supplementary Fig. 8. RNA-Seq analysis of K18-hACE2 mouse lungs with different pretreatments upon SARS-CoV-2 challenge.

a Bulk RNA-seq was conducted on lung homogenates from K18-hACE2 mice under mock treatment (n = 6) or post-viral challenge at 1, 2 and 4 dpi with each time point (n = 3). Pearson correlation analysis was executed on 27 samples using counts per million (CPM) data, with each cell displaying the Pearson correlation coefficient color-coded for visual ease. **b–f** GOBP enrichment analysis identifies biological processes enriched in up-regulated genes from comparisons at 1 (**b**), 2 (**c**), and 4 dpi (**d**) for PBS, 4 dpi for B5-D3 (**e**), and 4 dpi for B5-D3-LALA (**f**) versus the mock control, with top 15 significant terms displayed. *p*.adjust, adjusted *p* value; CAMKK, calmodulin-dependent protein kinase; AMPK, 5' adenosine monophosphate-activated protein kinase. Benjamin–Hochberg method was used for FDR adjustment.

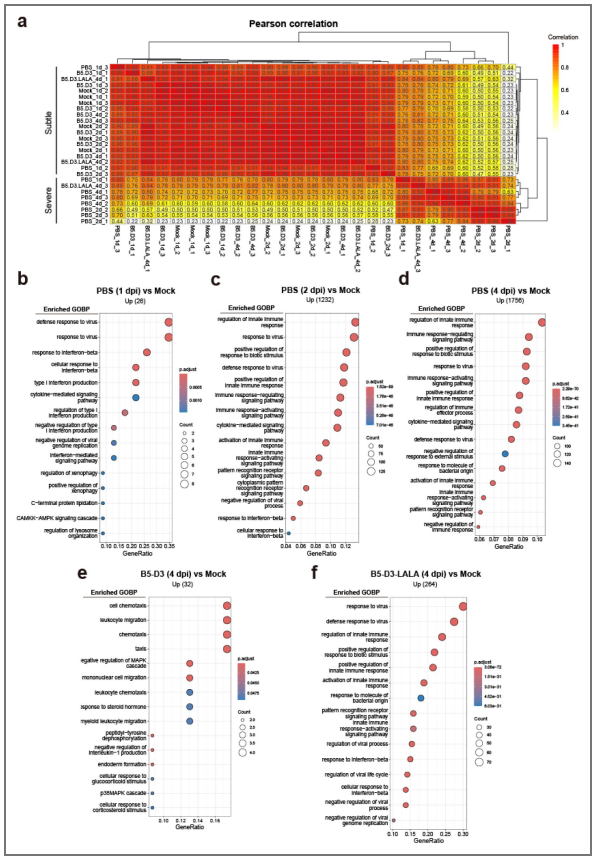

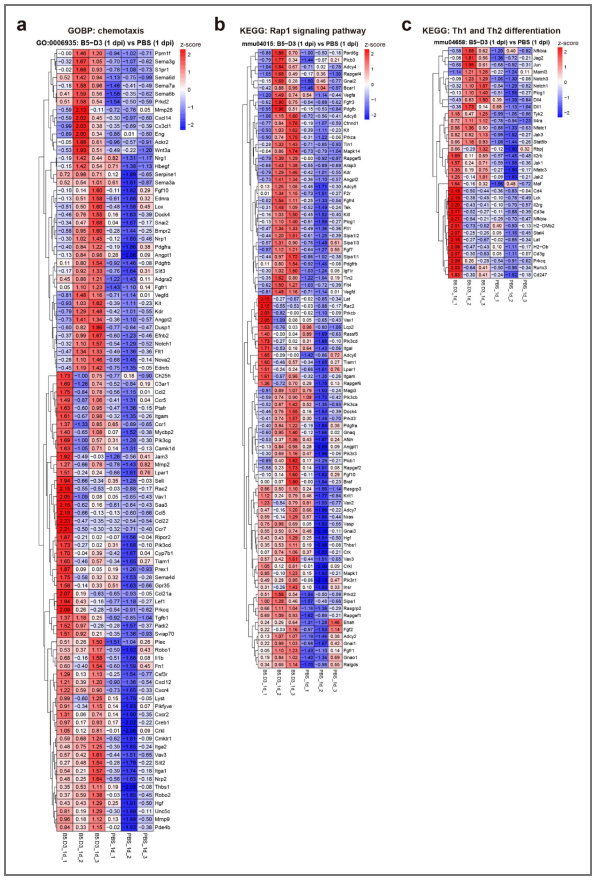

Supplementary Fig. 9. Leading-edge subsets in GSEA.

a–c Z-score plots show the relative level of gene expression in the leading edge subsets from GSEA comparing B5-D3 vs PBS at 1 dpi, corresponding to chemotaxis (**a**), Rap1 signaling pathway (**b**), and Th1 and Th2 differentiation (**c**).

Supplementary Fig. 10. Transcriptomic comparisons between B5-D3 and PBS pretreatments in K18-hACE2 mice upon SARS-CoV-2 challenge.

a, b DGE analysis between B5-D3 and PBS groups at 2 (**a**), and 4 dpi (**b**) showing up-regulated and down-regulated genes visualized in volcano plots. **c**, **d** GSEA of GOBPs significantly activated in B5-D3 groups compared to PBS groups at 2 dpi (**c**) and 4 dpi (**d**), with top 15 most significant terms displayed. **e, f** GSEA of KEGG pathways significantly activated in B5-D3 groups compared to PBS groups at 2 dpi (**e**) and 4 dpi (**f**), with all significant terms (**e**) and top 15 most significant terms (**f**) displayed. SFTS, Severe Fever with Thrombocytopenia Syndrome. Benjamin–Hochberg method was used for FDR adjustment.

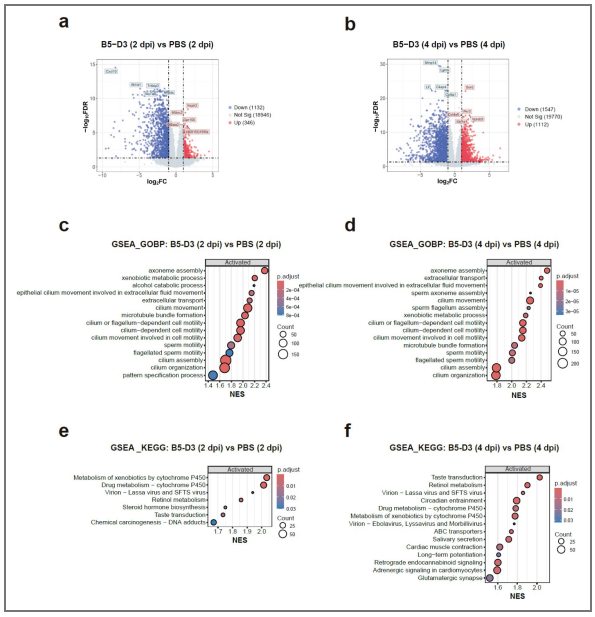

Supplementary Fig. 11. Minimal transcriptomic alterations in lungs after IN B5-D3 administration without viral challenge.

a Pearson correlation analysis for lung tissues collected 4 days post-administration of IN B5-D3 or PBS in female K18-hACE2 mice (n = 3), depicting correlation coefficients. **b** Volcano plot showing differentially expressed genes between the B5-D3 treated and control groups, with significant changes marked. **c** Venn diagram showing overlaps among the upregulated genes in **b** and in B5-D3 (4 dpi) in Fig. 4**c**.

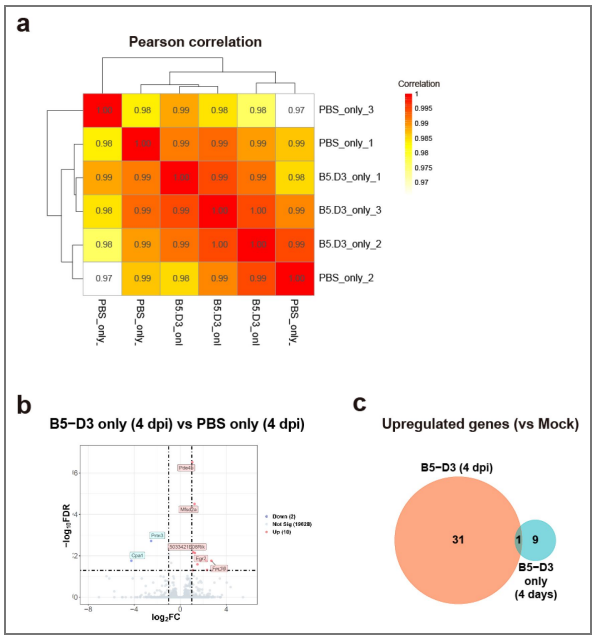

Supplementary Fig. 12. Flow cytometry analysis of mouse BALF cells.

a Flow cytometric gating strategy for BALF cells. **b** Percentages of individual cell types in CD45$^+$ BALF cells collected from individual animals. Ctrl group received no treatment before sacrifice.

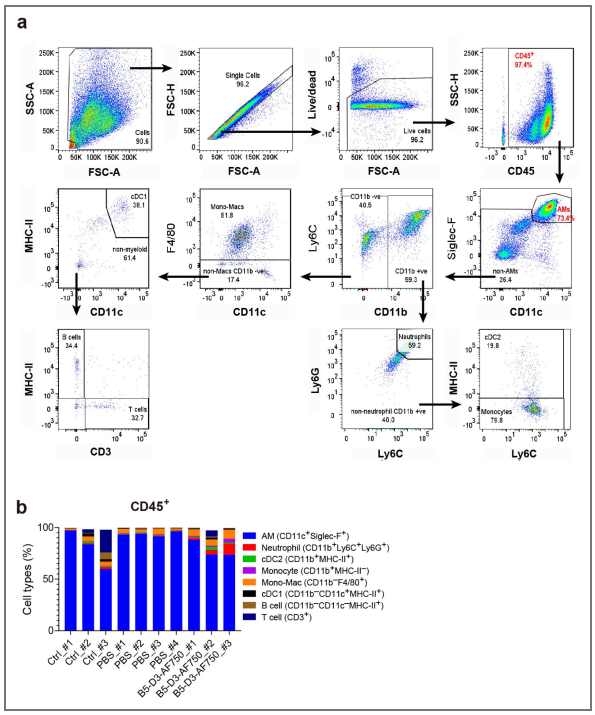

Supplementary Fig. 13. Binding/uptake rates of B5-D3-AF750 in BALF cells.

a–**f** Positive rates (left) and histograms (right) of B5-D3 binding/uptake as indicated by B5-D3-AF750 fluorescence intensities in CD11b$^+$Ly6C$^+$Ly6G$^+$ neutrophils (**a**), CD11b$^+$MHC-II$^+$ cDC2 (**b**), CD11b$^+$MHC-II$^-$ monocytes (**c**), CD11b$^-$CD11c$^+$MHC-II$^+$ cDC1 (**d**), CD11b$^-$CD11c$^-$MHC-II$^+$ B cells (**e**), and CD3$^+$ T cells (**f**). B5-D3$^+$ rates from individual mice are indicated on histograms. Data are presented as mean ± SEM, and statistical significance was determined by Student's t-test.

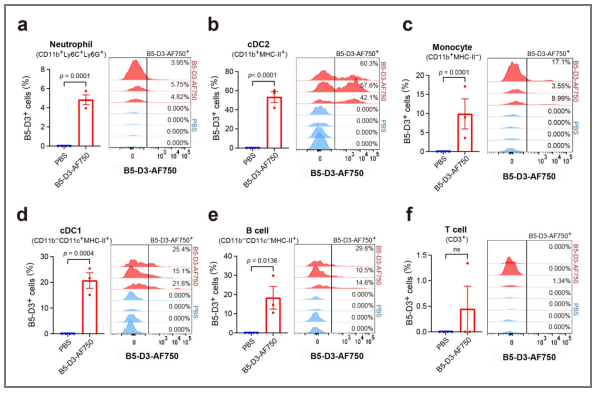

Supplementary Fig. 14. Time-course analysis of sACE2-Fc-dependent pseudovirus entry in THP-1 cells.

a Representative image showing B5-D3-mediated phagocytosis of pseudovirus by THP-1 monocytes at various time points (1, 3, 6, and 18 h). Cells were incubated with pseudovirus and B5-D3, followed by immunostaining for p24 (red, Invitrogen # PA5-81773). **b** Quantification of mean p24 signal intensity per cell as shown in **a**. IntDen per cell number indicates the average p24 signal per cell, analyzed using ImageJ. Each dot represents one image.

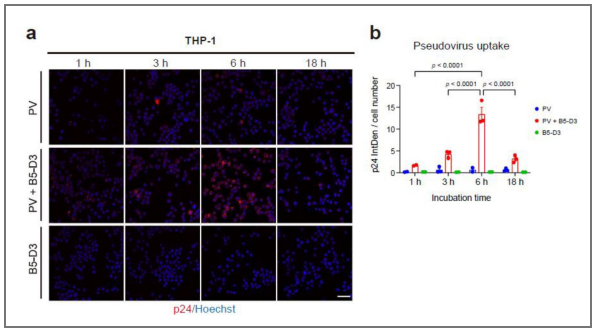

Supplementary Fig. 15. Enhanced phagocytosis of SARS-CoV-2 pseudovirus by THP-1 and THP-1-derived macrophages facilitated by sACE2-Fc.

a, **d** Representative images illustrating phagocytosis of SARS-CoV-2 pseudovirus by THP-1 monocytes (**a**) and THP-1 differentiated M1 macrophages (**d**) after 6 hours of incubation with or without sACE2-Fc (scale bar = 50 μm). p24 (Invitrogen # PA5-81773) and LAMP1 (Abcam # ab25630) were used to identify the pseudovirus and lysosomes, respectively. **b**, **e** Quantification of mean p24 signal intensity per cell for THP-1 monocytes (**b**) and M1 macrophages (**e**). IntDen per cell number indicates the mean p24 signal per cell, analyzed using ImageJ. Each dot represents one image. **c**, **f** Manders' coefficient demonstrating the colocalization of p24 and LAMP1 in THP-1 monocytes (**c**) and M1 macrophages (**f**). Data are presented as mean ± SEM, and statistical significance was determined by Tukey's multiple comparisons test.

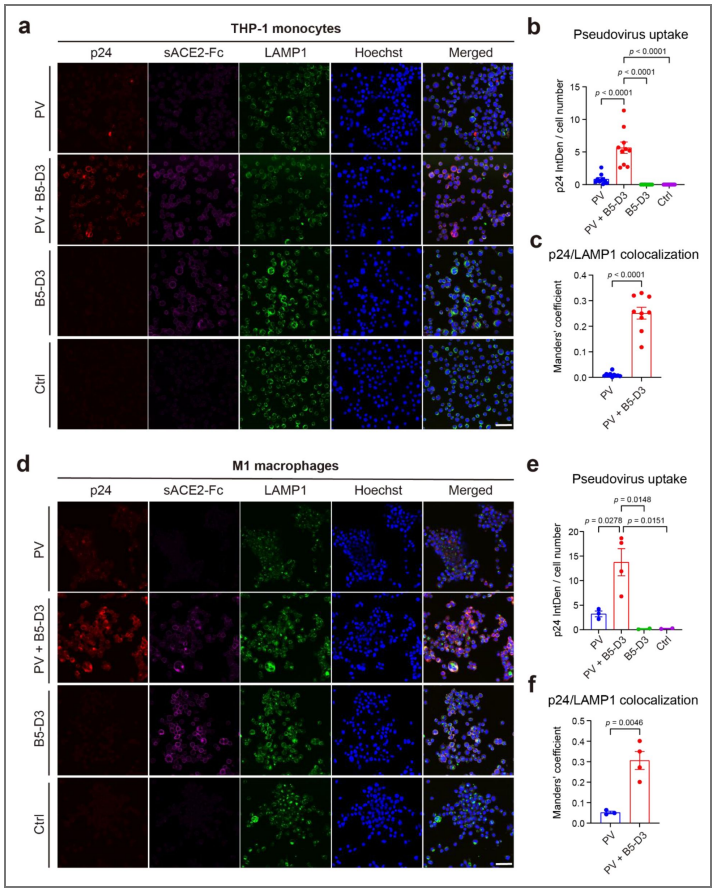

Supplementary Fig. 16. Generation of Calu-3 cell overexpressing hACE2 for enhanced pseudoviral infection.

a Immunostaining of hACE2 (Abcam # ab15348) in hACE2-Calu-3 and control Calu-3 cells. **b** Infection levels of SARS-CoV-2 pseudovirus in hACE2-Calu-3 versus control Calu-3 cells, quantified by luciferase assay 72 hours post-infection, performed in duplicate. Data are presented as mean ± SEM, and statistical significance was determined by Šídák's multiple comparisons test.

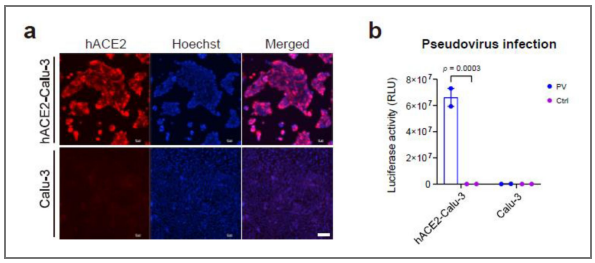

Supplementary Fig. 17. Reduced uptake of SARS-CoV-2 pseudovirus in THP-1-derived macrophages due to malfunction or absence of Fc domain in B5-D3.

a Representative images illustrating uptake of SARS-CoV-2 pseudovirus (PV) by THP-1-derived M1 macrophages at 6 h after incubation with B5-D3, B5-D3-LALA, and hIgG1 isotype with or without PV. Scale bar = 50 μm. **b** Quantification of mean p24 signal intensity per cell. IntDen per cell number indicates the mean p24 signal per cell, analyzed using ImageJ. Each dot represents one image. Data are presented as mean ± SEM, and statistical significance was determined by Tukey's multiple comparisons test.

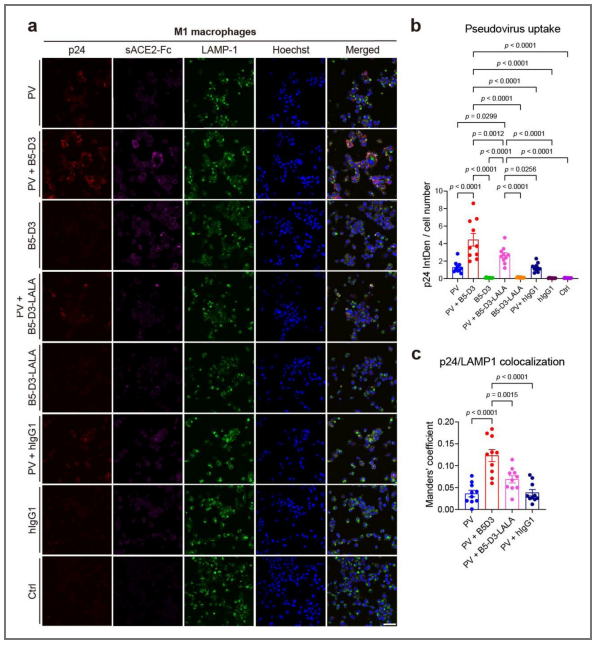

Supplementary Fig. 18. Transcriptomic analysis revealed activation of THP-1-derived macrophages mediated by 6 h incubation with B5-D3-pseudovirus complex.

a DGE analysis between THP-1-derived M0 macrophages incubated with B5-D3 + pseudovirus (PV) and those incubated with PV only (incubation time = 6 h). **b** GSEA of GOBPs significantly altered in the B5-D3 + PV group compared to the PV group, with top 15 most significantly activated and top 15 most significantly suppressed terms displayed. **c** GSEA of KEGG pathways significantly altered in the B5-D3 + PV group compared to the PV group, with top 15 most significantly activated and top 15 most significantly suppressed terms displayed. **d–i** GSEA plots of response to virus (**d**), response to type I interferon (**e**), JAK-STAT signaling pathway (**f**), MAPK signaling pathway (**g**), PI3K-Akt signaling pathway (**h**), and Rap1 signaling pathway (**i**) in B5-D3 + PV vs PV comparison. Benjamin–Hochberg method was used for FDR adjustment.

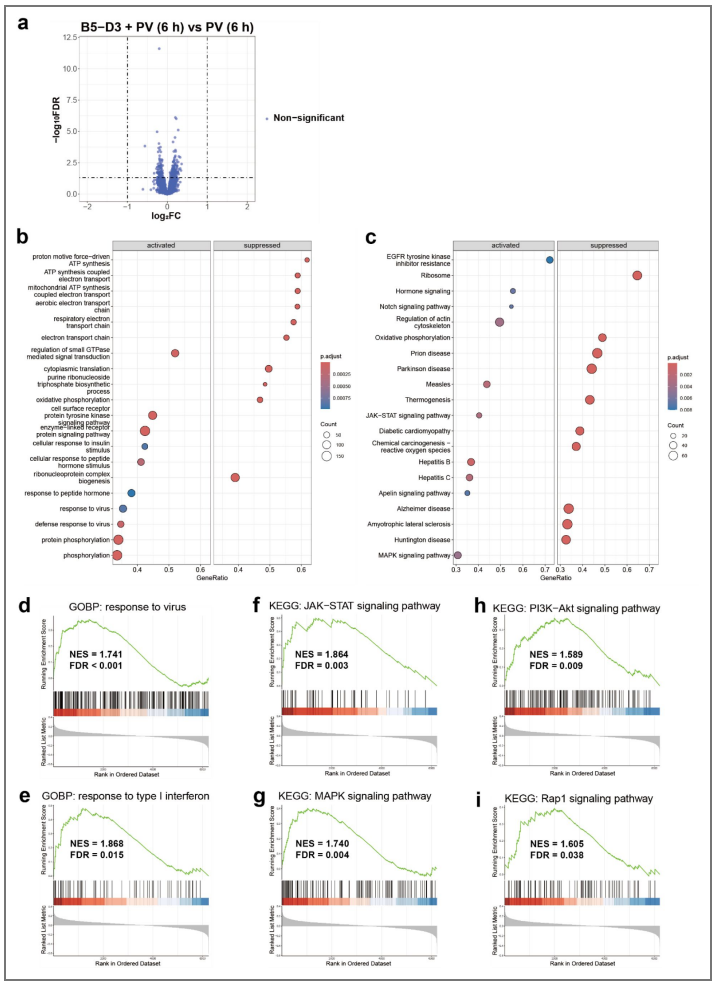

Supplementary Table 1. Enhanced tolerance and stability of B5-derivatives compared to WT sACE2-Fc in AAV-administered K18-hACE2 mice.

Detailed *post hoc* comparisons among treatment groups shown in Supplementary Fig. 4b. Diff., difference; **, $0.001 \le p < 0.01$; *, $0.01 \le p < 0.05$. *p* values were determined by Tukey's multiple comparisons test.

Tukey's multiple comparisons test	Mean Diff. (ng/mL)	Adjusted *p*	Summary
PBS vs. WT	-9990	0.0017	**
PBS vs. B5-D3	-29104	0.0046	**
PBS vs. B5-D4	-29894	0.0028	**
PBS vs. B5-D5	-26774	0.0013	**
WT vs. B5-D3	-19114	0.0145	*
WT vs. B5-D4	-19904	0.0078	**
WT vs. B5-D5	-16784	0.0021	**
B5-D3 vs. B5-D4	-790.4	0.9459	ns
B5-D3 vs. B5-D5	2330	0.4915	ns
B5-D4 vs. B5-D5	3120	0.2103	ns

Primers	Sequences
SARS-CoV-2 *S*	CGTCAGGCTGTTTAATAGGGGC
	GACTAGCTACACTACGTGCCCGC
SARS-CoV-2 *N*	CAATGGCGGTGATGCTGCTCTTG
	TTCTGGACCACGTCTGCCGAAAG
AAV copies	AGCCGGAGAACAACTACAAG
	CCAACACACAGATCTAATG
Mouse *Gapdh*	GGGCATCTTGGGCTACACTGAGGACCAG
	CACCCTGTTGCTGTAGCCGTATTCATTGTC

Supplementary Table 2. Primers used in quantitative PCR.

Data availability

All data associated with this study are available in the main text or the supplementary materials. The RNA-seq data generated in this study have been deposited in the NCBI Sequence Read Archive database under accession code PRJNA1054508. Constructs of diverse sACE2-Fc mutants and SARS-CoV-2 spikes are available upon request after completion and approval of a material transfer agreement by contacting fengbo@cuhk.edu.hk.

Acknowledgements

We thank the Chinese University of Hong Kong (CUHK) and the University of Hong Kong (HKU) research platforms for assistance in animal experimentation (the Laboratory Animal Service Center at CUHK and the Centre for Comparative Medicine Research at HKU) and histological analysis (Department of Pathology, HKU and Core Laboratory in the School of Biomedical Sciences, CUHK).

Additional information

Ethics approval and consent to participate

All animal procedures were ethically approved by The Chinese University of Hong Kong (CUHK)'s Animal Experimentation Ethics Committee (approval number: 20-226-MIS) and The University of Hong Kong (HKU)'s Committee on the Use of Live Animals in Teaching and Research (approval number: 5511-20).

Funding

This study was supported by Research Grants Council of Hong Kong grants 14115520, 14106024 (B.F.), C7145-20GF (L.L.P.), and in part by the Health@InnoHK Program launched by Innovation Technology Commission of the Hong Kong SAR, China. Jingyi W., J.L, B.L., and J.Q. received postgraduate studentships from the Chinese University of Hong Kong.

Authors' contributions

Jingyi W. and J.L. constructed the sACE2-Fc mutants and performed characterization analysis; A.W.C. performed the PRNTs and data analysis; Jingyi W., A.W.C., and J.L. performed the mouse infection experiments and data analysis; B.L., J.Q. and J.R. produced recombinant sACE2-Fc proteins; Jingyi W. and Junkang W. performed RNA-Seq analysis; Jingyi W. and J.Q. performed protein labeling, *in vivo* tracing of labeled protein, and flow cytometry analysis of BALF cells; J.L. performed THP-1 and Calu-3 experiments and confocal microscopic analysis. Junkang W. and J.L. performed protein structure prediction and visualization. Jingyi W., J.L., L.L.P. and B.F. conceived the project, designed experiments, and wrote the manuscript. Y.X., T.B., L.L.P. and B.F. revised the manuscript. All authors read and approved the final manuscript.

Funding

Funder	Grant reference number	Author
Research Grants Council, University Grants Committee	14115520	Bo Feng
Research Grants Council, University Grants Committee	14106024	Bo Feng
Research Grants Council, University Grants Committee	C7145-20GF	Leo LM Poon
Innovation and Technology Commission (ITC)	Health@InnoHK	Bo Feng

Chinese University of Hong Kong	Postgraduate studentship	Jiangchuan Li Jingyi Wang Bin Luo Jiale Qiu

Author ORCID iDs

Yin Xia: https://orcid.org/0000-0003-0315-7532
Thomas Braun: https://orcid.org/0000-0002-6165-4804
Leo LM Poon: https://orcid.org/0000-0002-9101-7953
Bo Feng: https://orcid.org/0000-0002-4018-3257

References

[1] **Wang Q.,** et al. (2023) Alarming antibody evasion properties of rising SARS-CoV-2 BQ and XBB subvariants. *Cell* **186**:279-286.e8 https://doi.org/10.1016/j.cell.2022.12.018 | PubMed

[2] **Hoffmann M.,** et al. (2020) SARS-CoV-2 Cell Entry Depends on ACE2 and TMPRSS2 and Is Blocked by a Clinically Proven Protease Inhibitor. *Cell* **181**:271-280.e8 https://doi.org/10.1016/j.cell.2020.02.052 | PubMed

[3] **Ozono S.,** et al. (2021) SARS-CoV-2 D614G spike mutation increases entry efficiency with enhanced ACE2-binding affinity. *Nature Communications* **12**:848 https://doi.org/10.1038/s41467-021-21118-2 | PubMed

[4] **Ramanathan M.,** Ferguson I. D., Miao W., Khavari P. A. (2021) SARS-CoV-2 B.1.1.7 and B.1.351 spike variants bind human ACE2 with increased affinity. *The Lancet Infectious Diseases* **21**:1070 https://doi.org/10.1016/S1473-3099(21)00262-0 | PubMed

[5] **Li L.,** et al. (2022) Structural basis of human ACE2 higher binding affinity to currently circulating Omicron SARS-CoV-2 sub-variants BA.2 and BA.1.1. *Cell* **185**:2952-2960.e10 https://doi.org/10.1016/j.cell.2022.06.023 | PubMed

[6] **Monteil V.,** et al. (2020) Inhibition of SARS-CoV-2 Infections in Engineered Human Tissues Using Clinical-Grade Soluble Human ACE2. *Cell* **181**:905-913.e7 https://doi.org/10.1016/j.cell.2020.04.004 | PubMed

[7] **Zoufaly A.,** et al. (2020) Human recombinant soluble ACE2 in severe COVID-19. *The Lancet Respiratory Medicine* **8**:1154-1158 https://doi.org/10.1016/S2213-2600(20)30418-5

[8] **Santos R. A. S.,** et al. (2018) The ACE2/Angiotensin-(1-7)/MAS Axis of the Renin-Angiotensin System: Focus on Angiotensin-(1-7). *Physiol Rev* **98**:505-553 https://doi.org/10.1152/physrev.00023.2016 | PubMed

[9] **Liu P.,** et al. (2018) Novel ACE2-Fc chimeric fusion provides long-lasting hypertension control and organ protection in mouse models of systemic renin angiotensin system activation. *Kidney International* **94**:114-125 https://doi.org/10.1016/j.kint.2018.01.029 | PubMed

[10] **Payandeh Z.,** et al. (2020) Design of an engineered ACE2 as a novel therapeutics against COVID-19. *Journal of Theoretical Biology* **505**:110425 https://doi.org/10.1016/j.jtbi.2020.110425 | PubMed

[11] **Lei C.,** et al. (2020) Neutralization of SARS-CoV-2 spike pseudotyped virus by recombinant ACE2-Ig. *Nature Communications* **11**:2070 https://doi.org/10.1038/s41467-020-16048-4 | PubMed

[12] **Glasgow A.,** et al. (2020) Engineered ACE2 receptor traps potently neutralize SARS-CoV-2. *Proceedings of the National Academy of Sciences* **117**:28046-28055 https://doi.org/10.1073/pnas.2016093117 | PubMed

[13] **Liu P.,** Xie X., Gao L., Jin J. (2020) Designed variants of ACE2-Fc that decouple anti-SARS-CoV-2 activities from unwanted cardiovascular effects. *Int J Biol Macromol* **165**:1626-1633 https://doi.org/10.1016/j.ijbiomac.2020.10.120 | PubMed

[14] **Chen Y.,** et al. (2022) Engineered ACE2-Fc counters murine lethal SARS-CoV-2 infection through direct neutralization and Fc-effector activities. *Science Advances* **8**:eabn4188 https://doi.org/10.1126/sciadv.abn4188 | PubMed

[15] **Hassler L.,** et al. (2023) Intranasal soluble ACE2 improves survival and prevents brain SARS-CoV-2 infection. *Life Science Alliance* **6**:e202301969 https://doi.org/10.26508/lsa.202301969 | PubMed

[16] **Kober D. L.,** et al. (2024) Development of a mutant aerosolized ACE2 that neutralizes SARS-CoV-2 *in vivo*. *mBio* **15**:e00768-24 https://doi.org/10.1128/mbio.00768-24 | PubMed

[17] **Chan K. K.,** et al. (2020) Engineering human ACE2 to optimize binding to the spike protein of SARS coronavirus 2. *Science* **369**:1261-1265 https://doi.org/10.1126/science.abc0870 | PubMed

[18] **Guy J. L.,** Jackson R. M., Jensen H. A., Hooper N. M., Turner A. J. (2005) Identification of critical active-site residues in angiotensin-converting enzyme-2 (ACE2) by site-directed mutagenesis. *The FEBS Journal* **272**:3512-3520 https://doi.org/10.1111/j.1742-4658.2005.04756.x | PubMed

[19] **Crawford K. H. D.,** et al. (2020) Protocol and Reagents for Pseudotyping Lentiviral Particles with SARS-CoV-2 Spike Protein for Neutralization Assays. *Viruses* **12**:513 https://doi.org/10.3390/v12050513 | PubMed

[20] **Korber B.,** et al. (2020) Tracking Changes in SARS-CoV-2 Spike: Evidence that D614G Increases Infectivity of the COVID-19 Virus. *Cell* **182**:812-827.e19 https://doi.org/10.1016/j.cell.2020.06.043 | PubMed

[21] **Suryamohan K.,** et al. (2021) Human ACE2 receptor polymorphisms and altered susceptibility to SARS-CoV-2. *Communications Biology* **4**:475 https://doi.org/10.1038/s42003-021-02030-3 | PubMed

[22] **Abramson J.,** et al. (2024) Accurate structure prediction of biomolecular interactions with AlphaFold 3. *Nature* **630**:493-500 https://doi.org/10.1038/s41586-024-07487-w | PubMed

[23] **Garcia-Beltran W. F.,** et al. (2021) Multiple SARS-CoV-2 variants escape neutralization by vaccine-induced humoral immunity. *Cell* **184**:2372-2383.e9 https://doi.org/10.1016/j.cell.2021.03.013 | PubMed

[24] **Mlcochova P.,** et al. (2021) SARS-CoV-2 B.1.617.2 Delta variant replication and immune evasion. *Nature* **599**:114-119 https://doi.org/10.1038/s41586-021-03944-y | PubMed

[25] **Kimura I.,** et al. (2022) The SARS-CoV-2 Lambda variant exhibits enhanced infectivity and immune resistance. *Cell Reports* **38**:110218 https://doi.org/10.1016/j.celrep.2021.110218 | PubMed

[26] **Halfmann P. J.,** et al. (2022) Characterization of the SARS-CoV-2 B.1.621 (Mu) variant. *Science Translational Medicine* **14**:eabm4908 https://doi.org/10.1126/scitranslmed.abm4908 | PubMed

[27] **Cao Y.,** et al. (2022) Omicron escapes the majority of existing SARS-CoV-2 neutralizing antibodies. *Nature* **602**:657-663 https://doi.org/10.1038/s41586-021-04385-3 | PubMed

[28] **Wang S.,** et al. (2023) Genomic Surveillance for SARS-CoV-2 - China, September 26, 2022 to January 29, 2023. *China CDC weekly* **5**:143-151 https://doi.org/10.46234/ccdcw2023.026 | PubMed

[29] **Amin R.,** Pal P., Dhama K., Emran T. B. (2023) Recent update on XBB.1.5 emerging novel mutation of COVID-19. *International Journal of Surgery* **109**:1048-1049 https://doi.org/10.1097/js9.0000000000000254 | PubMed

[30] **Weinreich D. M.,** et al. (2021) REGEN-COV Antibody Combination and Outcomes in Outpatients with Covid-19. *New England Journal of Medicine* **385**:e81 https://doi.org/10.1056/NEJMoa2108163 | PubMed

[31] **McCray P. B.,** et al. (2007) Lethal Infection of K18-*hACE2* Mice Infected with Severe Acute Respiratory Syndrome Coronavirus. *Journal of Virology* **81**:813-821 https://doi.org/10.1128/JVI.02012-06 | PubMed

[32] **Dwivedi V.,** et al. (2024) Age associated susceptibility to SARS-CoV-2 infection in the K18-hACE2 transgenic mouse model. *Geroscience* **46**:2901-2913 https://doi.org/10.1007/s11357-024-01102-6 | PubMed

[33] **Lund J.,** et al. (1991) Human Fc gamma RI and Fc gamma RII interact with distinct but overlapping sites on human IgG. *The Journal of Immunology* **147**:2657-2662 https://doi.org/10.4049/jimmunol.147.8.2657 | PubMed

[34] **Winkler E. S.,** et al. (2020) SARS-CoV-2 infection of human ACE2-transgenic mice causes severe lung inflammation and impaired function. *Nature Immunology* **21**:1327-1335 https://doi.org/10.1038/s41590-020-0778-2 | PubMed

[35] **Shan Q.,** et al. (2021) Tcf1 and Lef1 provide constant supervision to mature CD8+ T cell identity and function by organizing genomic architecture. *Nature Communications* **12**:5863 https://doi.org/10.1038/s41467-021-26159-1 | PubMed

[36] **Yamakita Y.,** et al. (2011) Fascin1 Promotes Cell Migration of Mature Dendritic Cells. *The Journal of Immunology* **186**:2850-2859 https://doi.org/10.4049/jimmunol.1001667 | PubMed

[37] **Colomer-Molera M.,** et al. (2023) Kv1.3-dependent immune system activation is regulated by KCNE4. *Biophysical Journal* **122**:14a https://doi.org/10.1016/j.bpj.2022.11.302

[38] **Rapp M.,** et al. (2019) CCL22 controls immunity by promoting regulatory T cell communication with dendritic cells in lymph nodes. *Journal of Experimental Medicine* **216**:1170-1181 https://doi.org/10.1084/jem.20170277 | PubMed

[39] **Korobova Z. R.,** Arsentieva N. A., Totolian A. A. (2023) Macrophage-Derived Chemokine MDC/CCL22: An Ambiguous Finding in COVID-19. *International Journal of Molecular Sciences* **24**:13083 https://doi.org/10.3390/ijms241713083 | PubMed

[40] **Katagiri K.,** Hattori M., Minato N., Kinashi T. (2002) Rap1 Functions as a Key Regulator of T-Cell and Antigen-Presenting Cell Interactions and Modulates T-Cell Responses. *Molecular and Cellular Biology* **22**:1001-1015 https://doi.org/10.1128/MCB.22.4.1001-1015.2002 | PubMed

[41] **Chanput W.,** Mes J. J., Wichers H. J. (2014) THP-1 cell line: An in vitro cell model for immune modulation approach. *International Immunopharmacology* **23**:37-45 https://doi.org/10.1016/j.intimp.2014.08.002 | PubMed

[42] **Tedesco S.,** et al. (2018) Convenience versus Biological Significance: Are PMA-Differentiated THP-1 Cells a Reliable Substitute for Blood-Derived Macrophages When Studying in Vitro Polarization?. *Frontiers in Pharmacology* **9** https://doi.org/10.3389/fphar.2018.00071 | PubMed

[43] **Takeda K.,** Akira S. (2005) Toll-like receptors in innate immunity. *International Immunology* **17**:1-14 https://doi.org/10.1093/intimm/dxh186 | PubMed

[44] **Yu S.,** et al. (2022) SARS-CoV-2 spike engagement of ACE2 primes S2' site cleavage and fusion initiation. *Proceedings of the National Academy of Sciences* **119**:e2111199119 https://doi.org/10.1073/pnas.2111199119 | PubMed

[45] **Urano E.,** et al. (2023) An inhaled ACE2 decoy confers protection against SARS-CoV-2 infection in preclinical models. *Science Translational Medicine* **15**:eadi2623 https://doi.org/10.1126/scitranslmed.adi2623 | PubMed

[46] **Ku Z.,** et al. (2021) Nasal delivery of an IgM offers broad protection from SARS-CoV-2 variants. *Nature* **595**:718-723 https://doi.org/10.1038/s41586-021-03673-2 | PubMed

[47] **Carabelli A. M.,** et al. (2023) SARS-CoV-2 variant biology: immune escape, transmission and fitness. *Nature Reviews Microbiology* **21**:162-177 https://doi.org/10.1038/s41579-022-00841-7 | PubMed

[48] **Cheemarla N. R.,** et al. (2021) Dynamic innate immune response determines susceptibility to SARS-CoV-2 infection and early replication kinetics. *Journal of Experimental Medicine* **218** https://doi.org/10.1084/jem.20210583 | PubMed

[49] **Senefeld J. W.,** et al. (2023) COVID-19 Convalescent Plasma for the Treatment of Immunocompromised Patients: A Systematic Review and Meta-analysis. *JAMA Network Open* **6**:e2250647-e2250647 https://doi.org/10.1001/jamanetworkopen.2022.50647 | PubMed

[50] **Gupta A.,** et al. (2021) Early Treatment for Covid-19 with SARS-CoV-2 Neutralizing Antibody Sotrovimab. *New England Journal of Medicine* **385**:1941-1950 https://doi.org/10.1056/NEJMoa2107934 | PubMed

[51] **Liu J.,** et al. (2023) An IgM-like inhalable ACE2 fusion protein broadly neutralizes SARS-CoV-2 variants. *Nat Commun* **14**:5191 https://doi.org/10.1038/s41467-023-40933-3 | PubMed

[52] **Guo H.,** et al. (2023) An ACE2 decamer viral trap as a durable intervention solution for current and future SARS-CoV. *Emerging Microbes & Infections* **12**:2275598 https://doi.org/10.1080/22221751.2023.2275598 | PubMed

[53] **Keyt B. A.,** Baliga R., Sinclair A. M., Carroll S. F., Peterson M. S. (2020) Structure, Function, and Therapeutic Use of IgM Antibodies. *Antibodies* **9**:53 https://doi.org/10.3390/antib9040053 | PubMed

[54] **Lutz C.,** Maher L., Lee C., Kang W. (2020) COVID-19 preclinical models: human angiotensin-converting enzyme 2 transgenic mice. *Hum Genomics* **14**:20 https://doi.org/10.1186/s40246-020-00272-6 | PubMed

[55] **Oladunni F. S.,** et al. (2020) Lethality of SARS-CoV-2 infection in K18 human angiotensin-converting enzyme 2 transgenic mice. *Nat Commun* **11**:6122 https://doi.org/10.1038/s41467-020-19891-7 | PubMed

[56] **Shu Y.,** McCauley J. (2017) GISAID: Global initiative on sharing all influenza data – from vision to reality. *Eurosurveillance* **22**:30494 https://doi.org/10.2807/1560-7917.ES.2017.22.13.30494 | PubMed

[57] **Lan J.,** et al. (2020) Structure of the SARS-CoV-2 spike receptor-binding domain bound to the ACE2 receptor. *Nature* **581**:215-220 https://doi.org/10.1038/s41586-020-2180-5 | PubMed

[58] **He X.,** et al. (2022) Low-dose AAV-CRISPR-mediated liver-specific knock-in restored hemostasis in neonatal hemophilia B mice with subtle antibody response. *Nature Communications* **13**:7275 https://doi.org/10.1038/s41467-022-34898-y | PubMed

[59] **Chen S.,** Zhou Y., Chen Y., Gu J. (2018) fastp: an ultra-fast all-in-one FASTQ preprocessor. *Bioinformatics* **34**:i884-i890 https://doi.org/10.1093/bioinformatics/bty560 | PubMed

[60] **Maulding N. D.,** Seiler S., Pearson A., Kreusser N., Stuart J. M. (2022) Dual RNA-Seq analysis of SARS-CoV-2 correlates specific human transcriptional response pathways directly to viral expression. *Scientific Reports* **12** https://doi.org/10.1038/s41598-022-05342-4 | PubMed

[61] **Kim D.,** Paggi J. M., Park C., Bennett C., Salzberg S. L. (2019) Graph-based genome alignment and genotyping with HISAT2 and HISAT-genotype. *Nature Biotechnology* **37**:907-915 https://doi.org/10.1038/s41587-019-0201-4 | PubMed

[62] **Love M. I.,** Huber W., Anders S. (2014) Moderated estimation of fold change and dispersion for RNA-seq data with DESeq2. *Genome Biology* **15** https://doi.org/10.1186/s13059-014-0550-8 | PubMed

[63] **Subramanian A.,** et al. (2005) Gene set enrichment analysis: A knowledge-based approach for interpreting genome-wide expression profiles. *Proceedings of the National Academy of Sciences* **102**:15545-15550 https://doi.org/10.1073/pnas.0506580102 | PubMed

[64] **Wu T.,** et al. (2021) clusterProfiler 4.0: A universal enrichment tool for interpreting omics data. *The Innovation* **2**:100141 https://doi.org/10.1016/j.xinn.2021.100141 | PubMed

Wang J, Li J (2023) Study of engineered soluble ACE2 decoys in protecting against SARS-CoV-2 in mice. NCBI Sequence Read Archive. ID PRJNA1054508 https://www.ncbi.nlm.nih.gov/bioproject/PRJNA1054508

Peer reviews

Reviewer #1 (Public review):

Summary:

This manuscript by Wang et al. describes the development of an optimized soluble ACE2-Fc fusion protein, B5-D3, for intranasal prophylaxis against SARS-CoV-2. As shown, B5-D3 conferred protection not only by acting as a neutralizing decoy, but also by redirecting virus-decoy complexes to phagocytic cells for lysosomal degradation. The authors showed complete in vivo protection in K18-hACE2 mice and investigated the underlying mechanism by a

combination of Fc-mutant controls, transcriptomics, biodistribution studies, and in vitro assays.

Strengths:

The major strength of this work is the identification of a novel antiviral approach with broad-spectrum and beyond simple neutralization. Mutant ACE2 enables broad and potent binding activity with the S proteins of SARS-CoV-2 variants, while the fused Fc part mediates phagocytosis to clear the viral particles. The conceptual advance of this ACE2-Fc combination is convincingly validated by in vivo protection data and by the completely abrogated protection of Fc LALA mutant.

Additionally:

The authors include a discussion (in Discussion part) about a previously reported ACE2 decamer (DOI: 10.1080/22221751.2023.2275598) and compared with the ACE2-Fc fusion protein developed in this study. The authors also tested the off-target activity and showed no evidence of toxicity in vivo.

https://doi.org/10.7554/eLife.108883.2.sa3

Reviewer #2 (Public review):

Summary:

Wang et al. engineered an ACE2 mutant by introducing two mutations (T92Q and H374N), and fused this ACE2 mutant to human IgG1-Fc (B5-D3). Experimental results suggest that B5-D3 exhibits broad-spectrum neutralization capacity and confers effective protection upon intranasal administration in SARS-CoV-2-infected K18-hACE2 mice. Transcriptomic analysis suggests that B5-D3 induces early immune activation in lung tissues of infected mice. Fluorescence-based bio-distribution assay further indicates rapid accumulation of B5-D3 in the respiratory tract, particularly in airway macrophages. Further investigation shows that B5-D3 promotes viral phagocytic clearance by macrophages via an Fc-mediated effector function, namely antibody-dependent cellular phagocytosis (ADCP), while simultaneously blocking ACE2-mediated viral infection in epithelial cells. These results provide some insights into improving decoy treatments against SARS-CoV-2 and other potential respiratory viruses.

Strengths:

The protective effect of this ACE2-Fc fusion protein against SARS-CoV-2 infection has been evaluated in a reasonable way.

Weaknesses:

(1) Some of the mice experiments suffer from insufficient sample numbers, which affect the statistical power and reliability of the results. The author acknowledged this weakness, noting that the supply of aged mice was limited, while arguing that, although the sample size is small, the data from these mice are consistent.

(2) Compared to 6 hours, intranasal administration of B5-D3 at 24 hours before viral infection results in reduced protective efficacy. However, only survival and body weight data are provided, with no supporting evidence from virological assays such as viral titer measurement. The author acknowledged that such data would be more comprehensive and attributed the limitation to constraints in animal services.

(3) The efficacy of the B5-D3-LALA group was not as good as that of the B5-D3 group. The author suggested that there might be a certain degree of viral variation, and viral infection in the lungs may be uneven in the B5-D3-LALA group.

https://doi.org/10.7554/eLife.108883.2.sa2

Reviewer #3 (Public review):

Strengths:

The core strength of this study lies in its innovative demonstration that an engineered sACE2-Fc fusion redirects virus-decoy complexes to Fc-mediated phagocytosis and lysosomal clearance in macrophages, revealing a distinct antiviral mechanism beyond traditional neutralization. Its complete prophylactic protection in animal models and precise targeting of airway phagocytes establish a novel therapeutic paradigm against SARS-CoV-2 variants and future respiratory viruses.

Weaknesses:

The study attributes the complete antiviral protection to Fc-mediated phagocytic clearance, a central claim that requires more rigorous experimental validation. The observation that abrogating Fc functions compromises protection could be confounded by potential alterations in the protein's stability, half-life, or overall structure. To firmly establish this mechanism, it is crucial to include a control molecule with a mutated Fc region that lacks FcγR binding while preserving the Fc structure itself. Without this critical control, the conclusion that phagocytic clearance is the primary mechanism remains inadequately supported. The strategy of deliberately targeting virus-decoy complexes to phagocytes via Fc receptors inherently raises the question of Antibody-Dependent Enhancement (ADE) of disease. While the authors demonstrate a lack of productive infection in macrophages, this only addresses one facet of ADE. The risk of Fc-mediated exacerbation of inflammation (ADE) remains a critical concern. The manuscript would be significantly strengthened by a direct discussion of this risk and by including data, such as cytokine profiling from treated macrophages, to more comprehensively address the safety profile of this approach. The exclusive use of the K18-hACE2 mouse model, which exhibits severe disease, limits the generalizability of the findings. The "complete protection" observed may not translate to models with more robust and naturalistic immune responses or to human physiology. Furthermore, the lack of data against circulating SARS-CoV-2 variants of concern. The concept of sACE2-Fc fusion proteins as decoy receptors is not novel, and numerous similar constructs have been previously reported. The manuscript would benefit from a clearer demonstration of how the optimized B5-D3 mutant represents a significant advance over existing sACE2-Fc designs. A direct comparative analysis with previously published benchmarks, particularly in terms of neutralizing potency, Fc effector function strength, and in vivo efficacy, is necessary to establish the incremental value and novelty of this specific agent.

Comments on revised version:

The author has successfully addressed the raised issue.

https://doi.org/10.7554/eLife.108883.2.sa1

Author response:

The following is the authors' response to the original reviews.

> ***Public Reviews:***
>
> ***Reviewer #1 (Public review):***
>
> *Summary:*

> *This manuscript by Wang et al. describes the development of an optimized soluble ACE2-Fc fusion protein, B5-D3, for intranasal prophylaxis against SARS-CoV-2. As shown, B5-D3 conferred protection not only by acting as a neutralizing decoy, but also by redirecting virus-decoy complexes to phagocytic cells for lysosomal degradation. The authors showed complete in vivo protection in K18-hACE2 mice and investigated the underlying mechanism by a combination of Fc-mutant controls, transcriptomics, biodistribution studies, and in vitro assays.*
>
> *Strengths:*
>
> *The major strength of this work is the identification of a novel antiviral approach with broad-spectrum and beyond simple neutralization. Mutant ACE2 enables broad and potent binding activity with the S proteins of SARS-CoV-2 variants, while the fused Fc part mediates phagocytosis to clear the viral particles. The conceptual advance of this ACE2-Fc combination is convincingly validated by in vivo protection data and by the completely abrogated protection of Fc LALA mutant.*

We thank the reviewer for his recognition and positive comments on our study.

> *Weaknesses:*
>
> *Some aspects could be further modified.*
>
> *(1) A previously reported ACE2 decamer (DOI: 10.1080/22221751.2023.2275598) needs to be mentioned and compared in the Discussion part.*

We thank the reviewer for pointing out this weakness.

Indeed, previous studies reported that the ACE2-IgM decamer, taking advantage of the decameric structure of IgM, exhibited higher avidity to spikes and greater potency for viral neutralization [1-3]. In particular, the study by Guo et al. has demonstrated a broad-spectrum neutralization ability of the ACE2-IgM decamer against multiple SARS-CoV-2 variants and reported the efficacy of intranasal prophylaxis in preventing lethal SARS-CoV-2 challenge in K18-hACE2 mice.

We agree with the reviewer that it is promising that our B5-D3 design would benefit from switching to the IgM isotype. However, the distinct biological features imposed by IgM Fc, including short serum half-life and restricted tissue penetration [4], may complicate the study design and diverge our focus.

In our current study, we would focus on the IgG1 Fc-based decoy design, while inactivating the enzyme activity of ACE2 to avoid disturbing the renin angiotensin system. This design allowed us to compare diverse administration routes and regimens and to gain useful insights into the potential of sACE2-Fc decoy in combating SARS-CoV-2 *in vivo*.

We appreciated the reviewer‘s insightful suggestion. In the revised manuscript, we have included additional discussion regarding ACE2-IgM decamer, addressing the relevant concern on page 17 lines 409–414.

> *(2) Limitations of this study, such as off-target binding and potential immunogenicity, should also be discussed.*

We thank the reviewer for his insightful comments and agree that off-target activity is a major concern for designing the ACE2 decoy.

(1) In our study, the representative sACE2-Fc decoy candidate B5-D3 contains H374N mutation (D3) that is designed to inactivate ACE2 enzyme activity by causing dyscoordination of Zn2+. Our *in vitro* enzymatic activity assay has demonstrated that the H374N mutation (D3), as well

as other three single mutations D1, D4 and D5, in either WT sACE2-Fc or B5 mutant, could effectively abolish the hACE2 enzyme activity (Supplementary Fig. 2e, h).

(2) To further address the concern on off-target activity, we performed AAV-based overexpression experiments in K18-hACE2 mice and examined serum levels of RAS hormones, using ELISA methods that specifically detect serum renin, Angiotensin II (Ang II), and Ang (1-7). While our data from WT sACE2-Fc overexpression revealed significantly elevated serum renin and Ang II, indicating a disruption of the RAS (Supplementary Fig. 4d, e); the results from examined double mutants, including B5-D3, showed negligible change in any of these metabolite levels, demonstrating no off-target effect and minimal disturbance to the RAS activity in K18-hACE2 mice (Supplementary Fig. 4d–f).

(3) Moreover, in this experiment, after the prolonged overexpression of all these molecules in K18hACE2 mice, histological examination of multiple organs showed no evidence of immune cell infiltration and tissue damage and no difference was observed between the mice receiving WT sACE2-Fc or B5-D3(Supplementary Fig. 4g).

In the revised manuscript, we have included the results from the AAV-delivered *in vivo* overexpression of WT sACE2-Fc and three most promising double mutants (B5-D3, B5-D4 and B5-D5) on page 5 lines 118–122 and on page 6 lines 123–135 in the main text. The relevant data were presented in the new Supplementary Fig. 4.

> ***Reviewer #2 (Public review):***
>
> *Summary:*
>
> *Wang et al. engineered an optimized ACE2 mutant by introducing two mutations (T92Q and H374N) and fused this ACE2 mutant to human IgG1-Fc (B5-D3). Experimental results suggest that B5-D3 exhibits broad-spectrum neutralization capacity and confers effective protection upon intranasal administration in SARS-CoV-2-infected K18-hACE2 mice. Transcriptomic analysis suggests that B5D3 induces early immune activation in lung tissues of infected mice. Fluorescence-based biodistribution assay further indicates rapid accumulation of B5-D3 in the respiratory tract, particularly in airway macrophages. Further investigation shows that B5-D3 promotes viral phagocytic clearance by macrophages via an Fc-mediated effector function, namely antibody-dependent cellular phagocytosis (ADCP), while simultaneously blocking ACE2-mediated viral infection in epithelial cells. These results provide insights into improving decoy treatments against SARS-CoV-2 and other potential respiratory viruses.*
>
> *Strengths:*
>
> *The protective effect of this ACE2-Fc fusion protein against SARS-CoV-2 infection has been evaluated in a quite comprehensive way.*

We thank the reviewer for his recognition and positive comments on our study.

> *Weaknesses:*
>
> *(1) The paper lacks an explanation regarding the reason for the combination of mutations listed in Supplementary Figure 2b. For example, for the mutations that enhance spike protein binding, B2-B6 does not fully align with the mutations listed in Table S1 of Reference 4, yet no specific criteria are provided.*

We thank the reviewer for pointing out this negligence.

We constructed the B2-B6 mutants based on the study by Chan et al. [5] (Reference 4 in the previous version), mainly referencing to their Fig. 1A rather than to their Table S1. In Chan's study, each of the proposed mutations were discovered as single mutations in monomeric

sACE2 molecules based on the enrichment in target cell-binding. T92 was a notable hot spot for enriched mutations in their Fig. 1A.

Since monomeric and dimeric forms of sACE2 showed dramatically different kinetics for ACE2-RBD interaction, we selected five proposed mutations and further examined their affinity and activity in dimeric sACE2-Fc in our study. We chose not only the combinations of mutations, such as B3, B4, and B6 proposed in their Table S1, but also explored less-complicated mutation(s) like B2 (T27Y/L79T) and B5 (T92Q) in their Fig. 1A, which were *in silico* predicted to enhance ACE2-RBD binding but not tested in sACE2-Fc in Chan's study.

Interestingly, although our results confirmed enhanced viral neutralization by all these mutations, the activity increase compared to WT ACE2-Fc was rather limited. Hence, we chose not to explore other mutations but to focus on B2–B6 to construct an enhanced ACE2-Fc decoy as a representative, to investigate the potential of ACE2-Fc decoys in combating SARS-CoV-2 infections.

In the revised manuscript, we have further amended the writing on page 4 lines 84–87 to enhance the readability. Whereas for conciseness of the manuscript, we did not describe in too much detail how we selected the mutations to be tested.

> *Second, for the mutations that abolished enzymatic activity, while D1 and D2, D3, D4, and D5 are cited from References 12, 11, and 33, respectively, the reason for combining D3 and D4 into A2, and D1 and D2 into A3 remains unexplained. It is also unclear whether some of these other possible combinations have been tested. Furthermore, for the B5-derived mutations, only double-mutant combinations with D1-D5 are tested, with no attempt made to evaluate triple mutations involving A2 or A3.*

We thank the reviewer for pointing out this negligence.

A2 and A3 mutations were originally proposed as double mutations [6,7]. A2 (H374N/H378N) was first reported by Guy et al. [6] (Reference 11 in the previous version), while A3 (R273G/T445G) was originally proposed in Payandeh et al.'s study [7] (Reference 33 in the previous version).

In this study, we further split the two mutations in A2 and A3, to generate the single enzymedeactivating mutations, D1 and D2 from A3, and D3 and D4 from A2. Among these single mutations, D2 failed to inactivate ACE2 enzymatic activity (Supplementary Fig. 2e), and it was excluded in subsequent analyses.

D5 (H345L) was a single mutation directly adopted from the report by Glasgow et al. [8] (Reference 12 in the previous version).

After combining the B5 with the enzyme-deactivating mutations (A2, A3, D1, D3, D4, D5), our neuralization assay results showed that, the simpler compound mutants with only two mutations, like B5-D1, B5-D3, B5-D4 and B5-D5, exhibited stronger neutralization capacity than B5-A2 and B5-A3 with triple mutations. Moreover, since fewer mutations were more favorable to reduce risks in causing protein structure alteration and evoking host immunity, we then focused on the sACE2-Fc double mutants B5-D3, B5-D4 and B5-D5 in the subsequent neutralization and overexpression assays (Supplementary Fig. 3 and 4), and examined B5-D3 as a representative candidate in the *in vivo* infection tests and follow-up analysis (Figure 2–6, and Supplementary Figures 5–18).

We agree that the lack of explanation for splitting A2 and A3 into D1 to D4 single mutations made the rationale unclear. In the revised manuscript, we have included our previous test results on B5-A2 and B5-A3, cited Lei et al.'s study using A2 in ACE2 decoy [9], and explained the rationale for splitting A2 and A3 into D1 to D4 mutations. Relevant revision was made on

page 4 lines 94–97 in the main text, while the design and data for B5-A2 and B5-A3 were included in the revised Figure 1b and Supplementary Figure 2b, f–h.

> *(2) Figures 1b, 1d, and 1e lack statistical analyses, making it difficult to determine whether B5 and D3 exhibit significant advantages. For Wuhan-Hu-1 strain, B2 and B5 are similar, and for D614G strain, B2, B3, B4, B5, and B6 display comparable results. However, only the glycosylation-related single mutant B5 is chosen for further combinatorial constructs. Moreover, for VOC/VOI strains, B5 is superior to B5-D3; for the Alpha strain, B5-D4 and B5-D5 are superior to B5-D3; and for the Delta and Lambda strains, B5-D5 is superior to B5-D3. These observations further highlight the need for a clearer explanation of the selection strategy.*

We agree with the reviewer's insightful observations.

Indeed, although our results confirmed enhanced viral neutralization by these reported mutations, the activity increases compared to WT ACE2-Fc were generally limited. Importantly, these observations were largely consistent with other reports (including the study by Chan et al. [5]), suggesting limited potential of mutagenesis in enhancing the ACE2-RBD/Spike interaction. Therefore, we chose to selectively examine B2-B6 to construct an enhanced ACE2-Fc decoy with reasonable performance, as a representative candidate to study the application potential of ACE2-Fc decoy.

The IC_{50} values in Figures 1b, 1d, and 1e were calculated from neutralization curves, measuring infection reduction at multiple concentrations in duplicates, which therefore were presented with statistical support. Based on the multiple neutralization assays, B5-D3 consistently showed a high performance among other top-performers (Figure 1, Supplementary Fig. 2f,g, and Supplementary Fig. 3).

We agree that B2 and B5 performed comparably well in neutralization assays, but B2 contains two mutations (T27Y/T92Q) while B5 carries a single mutation (T92Q). Hence, we decided to focus on B5 due to its lowest mutational burden and least potential risk.

We agree that for VOC/VOI strains, B5 was superior to B5-D3 in pseudovirus-neutralization assays. However, B3-D3 was enzymatically inactive, which is essential for generating safe ACE2 decoy and, therefore, justifies our usage of B5-D3 over B5.

We agree with the reviewer that, altogether, the B5-D3 did not show significant advantages than other top performers like B5-D4 and B5-D5. Here, B5-D3 was selected as a representative, which performed equally well rather than being the most outstanding candidate, for subsequent examination of efficacy, safety, and mechanistic insights.

We thank the reviewer for his valuable feedback. In the revised manuscript, we have further amended our description of B5-D3, as a "representative" candidate, to improve the readability. Relevant changes can be found on page 4 line 84, page 5 line 109, page 14 line 333 and page 15 line 360.

> *(3) Figure 1e does not specify the construct form of the control hIgG1, namely whether it is an hIgG1 Fc fragment or a full-length hIgG1 protein. If the full-length form is used, the design of its Fab region should be clarified to ensure the accuracy and comparability of the experimental control.*

We thank the reviewer for pointing out this negligence.

In this study, we used the *in vivo* grade recombinant human IgG1 isotype control antibody in its full length (Syd labs, #PA007125) as the negative control. It is the 4F17 clone, which is widely used and showed low or no specific binding to any human samples [10] (Human IgG1

Isotype Control Antibody | Recombinant, *in vivo* Grade - Syd Labs). We have added the relevant information in the MATERIALS AND METHODS on page 23 lines 548–549.

> *(4) In Figure 2a, all three PBS control mice died, whereas in Figure 2f, three out of five PBS control mice died, with the remaining showing gradual weight recovery. This discrepancy may reflect individual immune variations within the control groups, and it is necessary to clarify whether potential autoimmune factors could have affected the comparability of the results. Also, the mouse experiments suffer from insufficient sample sizes, which affects the statistical power and reliability of the results. In Figure 2a, each group contains only 4 replicates, one of which was used for lung tissue sampling. As a result, body weight monitoring data is derived from only 3 mice per group (the figure legend indicating n=4 should be corrected to n=3). Such a small sample size limits the robustness of the conclusions. Similarly, in Figure 2f, although each group has 5 replicates, body weight data are presented for only 4 mice, with no explanation provided for the exclusion of the fifth mouse. Furthermore, the lung tissue experiments in Figure 3a include only 3 replicates, which is also inadequate.*

We thank the reviewer for his valuable feedback.

Figure 2a was the first *in vivo* infection experiment of this study, and we performed the test in aged female K18-hACE2 mice at 10–12 months old. Whereas for the subsequent experiments in Figure 2f and Figure 3, we changed to young female K18-hACE2 mice at 2–3 months old, because the limited supply of old mice. While in Figure 2a, four aged mice (not three) in the PBS control group all died within 7 dpi, results of Figure 2f and Figure 3 consistently showed heterogeneous responses among young mice in the PBS control groups. Since increased susceptibility to SARS-CoV-2 infection has been broadly observed among aged human populations and it was also supported by mouse study [11], here we would attribute the observed discrepancy to the age difference between the two cohorts in Figure 2a and 2f. In the revised manuscript, we have further elucidated this observation in results (on page 7 lines 163–167) and included a new reference for better clarification (page 7 line 167).

Furthermore, because the PBS control mice in both Figure 2a and 2f died within 7 dpi, which was too soon for autoimmune factors to take place. Moreover, we have performed AAV-based prolonged overexpression experiments in K18-hACE2 mice (new Supplementary Fig. 4), which showed no tissue damage in either WT sACE2-Fc or B5-D3 treated mice, suggesting low immunogenicity. Collectively, the autoimmune factors are unlikely the reason leading to the different survival between PBS controls in Figure 2a and 2f.

We thank the reviewer for pointing out the weakness regarding small sample sizes in our study.

(1) In Figure 2a–c, the experiment was performed in an aged cohort at 10–12 months old, starting with 5 mice in each virus-inoculated group and 4 mice in the mock control group. At 4 dpi, we sacrificed one mouse from each group for tissue analysis. Therefore, in the survival analysis, there were 4 mice in each virus-inoculated group and 3 mice in the mock control group, whose survival and body weight changes were presented in Figure 2b, c.

Despite the relatively small sample sizes in Figure 2b, c, all 4 PBS control mice died, while all 4 mice in 6-hour B5-D3 IN prophylaxis group survived, demonstrating 100% survival and no sign of body weight loss. The survival and body weight data were highly consistent, strongly supporting that B5-D3 intranasal prophylaxis could protect the mice from lethal SARS-CoV-2 infection.

To enhance clarity, in the revised manuscript, we have added the sample size information in chart legends in Figure 2a–c.

(2) In Figure 2f–h, the experiment was performed in a young cohort at 2–3 months old and the body weight and survival data were presented for 5 mice in each group (not for 4 mice). Notably, although 2 out of 5 young mice in the PBS control group eventually survived from the viral infection, they had suffered significant weight loss during 4–7 dpi, similarly to the died. Whereas all 5 mice in the – 6hr B5-D3 IN prophylaxis group showed no sign of weight loss. Hence, these data were highly consistent with Figure 2b, c, supporting the efficiency of B5-D3 IN prophylaxis in protection against SARS-CoV-2 infection.

We noticed that some data points in Figure 2g, h were very close to each other, making it difficult to distinguish the data line for individual mice. To enhance clarity, in the revised manuscript, we have added sample-size information in chart legends in Figure 2g and 2h.

(3) In Figure 3a, we aimed to examine the lung tissues at early time points. For each treatment, we have 3 mice sacrificed at a single selected time point. Hence, total 9 mice were examined in the PBS control group and B5-D3 IN group, yielding results at 1 dpi, 2 dpi and 4 dpi that consistently supported each other. Moreover, the viral titers, S, and N protein expression analysis all showed significant difference among different groups. Therefore, our experiments have enough discrepancy between different treatment groups to draw the conclusion.

> *(5) Compared to 6 hours, intranasal administration of B5-D3 at 24 hours before viral infection results in reduced protective efficacy. However, only survival and body weight data are provided, with no supporting evidence from virological assays such as viral titer measurement. Therefore, the long-term effectiveness lacks sufficient experimental validation.*

In Figure 2f–h, we aimed to compare the efficacies of IN administration of B5-D3 at different timepoints, mainly focusing on the body weight change and survival data along the infection and recovery time. As indicated by early data in Figure 2d, viruses were largely cleared by 4 dpi in mice treated with B5-D3 prophylaxis. Therefore, in this test, we did not examine virus titers in the recovered animals by the end of observation at 14 dpi. Instead, we examined plasma levels of virus-neutralizing antibodies in the survivors at the endpoint, which indeed supported that the 6-hours and 24-hours IN B5-D3 prophylaxis provided effective protection against the SARS-CoV-2 infection and resulted in minimal levels of neutralizing antibodies in plasma, as shown in Figure 2i.

Collectively, the body weight, survival, and antibody data all supported that 6-hour IN B5-D3 prophylaxis achieved the best efficacy. Hence, we performed comprehensive viral titer and profiling analysis at early time points like 1 dpi, 2 dpi, and 4 dpi, focusing only on the 6-hour IN B5-D3 prophylaxis. This works also included B5-D3-LALA control to examine viral titers, host immune responses, and underlying mechanisms (Figure 3,4).

We agree with the reviewer that it would be more comprehensive if our experiments could include indepth analysis of the 24-hours IN B5-D3 prophylaxis group. However, due to limited capacity of animal service, we chose to focus on the best-performing group as a representative treatment to study the underlying mechanisms.

> *(6) In Figures 3b and 3c, viral spike (S) and nucleocapsid (N) RNA relative expression levels are quantified by qPCR. The results show significant individual variation within the B5-D3-LALA treatment group: one mouse exhibits high S and N expression, while the other two show low expression. Viral load levels are also inconsistent: two mice have high viral loads, and one has a low viral load. Due to this variability, the available data are insufficient to robustly support the conclusion.*

We understand the reviewer's concern on the variability within the B5-D3-LALA group. However, we have some reservations about the importance of further increasing the sample

sizes in this test.

First, since viral gene transcription and viral particle levels represented different phases in viral life, they may follow different kinetics during infection progression and lead to variability. Second, we used different parts of the lung tissues from each mouse for extracting RNA and tissue homogenates, which were then used for detection of S/N expression and viral load levels, respectively. The uneven viral infection in the lung might also contribute to the variability. Furthermore, in this test, both our qPCR and viral load analysis data consistently demonstrated that the B5-D3-LALA was less effective than B5-D3, indicating that Fc function played an important role in supporting full protection by B5-D3 against lethal SAS-CoV-2 infections. This observation is also supported by other studies [12].

We appreciate the valuable feedback from the reviewer. In the revised manuscript, we have further clarified these observations on page 8, lines 192–194, and included alveolar thickening data on page 9, lines 202–204.

> *(7) Figure 3e: "H&E staining indicated alveolar thickening in all groups," including the Mock group. Since the Mock group did not receive virus or active drug treatment, this observed change may result from local tissue reaction induced by the intranasal inoculation procedure itself, rather than specific immune activation. A control group (no manipulation) should be set to rule out potential confounding effects of the experimental procedure on tissue morphology, thereby allowing a more accurate assessment of the drug's effects.*

We thank the reviewer for his insightful comments and suggestions.

We have further examined our H&E staining and quantified alveolar thickening in different treatment groups. Indeed, the data suggested a transient alveolar thickening in the mock group at 1 dpi, which was improved at 2 dpi. This observation supports that the intranasal procedure itself indeed caused a transient alveolar thickening, that was evident at 1 dpi but disappeared at 2 dpi.

Notably, moderate alveolar thickening was found to be persistent in the B5-D3-treated mice till the end point at 4 dpi. Whereas the PBS groups with intensive SARS-CoV-2 infection progressively developed severe structural damage and showed much stronger alveolar thickening than B5-D3 or mock groups at 4 dpi. Consistent with the partial protection by B5-D3-LALA, histological analysis of lung samples in this group revealed severer yet heterogenous alveolar thickening. These observations suggested that -6h IN B5-D3 treatment prevented tissue damage brought by infection with minimal yet efficient immune activation.

In the revised manuscript, we have included the quantitation results of alveolar thickening on page 9, lines 200–204 and presented the data in new Supplementary Fig. 7.

> *(8) In Supplementary Figure 11b, a considerable number of alveolar macrophages (AMs) are observed in both the PBS and B5-D3 groups. This makes it difficult to determine whether the observed accumulation is specifically induced by B5-D3.*

We thank the reviewer for pointing out this issue.

In this experiment, the cell populations examined in previous Supplementary Fig. 11b and Fig. 5h are different, though graphs appear similar.

Supplementary Fig. 11b (new Supplementary Fig. 12b) showed the analysis among CD45+ immune cells, regardless of B5-D3-AF750 signal. The dominance of AMs among immune cell populations is a normal physiological feature of BALF cells. To make this clear, we have added new data of BALF cells from untreated mice in the revised manuscript and new Supplementary Fig. 12b.

Fig. 5h displayed for cell type analysis among the CD45+ B5-D3-AF750+ cells —only CD45+ immune cells that took up the AF750-labeled B5-D3.

To enhance clarity, in the revised manuscript, we have amended the labels as CD45+ B5-D3-AF750+ in Figure 5h (and similarly in revised Supplementary Fig. 13), to differentiate the data from that in CD45+ cells shown in the revised Supplementary Fig. 12b.

> *(9) In the flow cytometry experiment shown in Figure 5, the PBS control group is not labeled with AF750, which necessarily results in a value of zero for "B5-D3+ cells" on the y-axis. An appropriate control (e.g., hIgG1-Fc labeled with AF750) should be included.*

We thank the reviewer for his valuable question.

In this experiment, we intended to analyze all immune cells with positive AF750 signals, to identify the major immune cell types that took up AF750-B5-D3 as the candidate cells responsible for the observed activation of innate immunity. Hence, here we deliberately set PBS vehicle treatment without AF750 signal as the control group for gating.

This analysis aimed to provide an overall picture of immune cell types that actively take up ACE2 decoy, likely via Fc receptor-mediated binding. Control IgG1 labeled with AF750, with an Fc region, may show similar profile and biodistribution among BALF immune cells, which, therefore, was not examined as control for gating.

Instead, in the revised manuscript, we have added new analysis results comparing the efficiencies of B5-D3 and IgG1 in mediating pseudovirus uptake in THP-1-derived macrophages. IgG1 isotype control was examined to address ACE2-specific effect. Indeed, we observed no pseudovirus uptake based on p24 signal, in the IgG1 treated samples, indicating that the presence of B5-D3 is crucial for efficient pseudovirus uptake in macrophages due to the sACE2-spike affinity. These results have been added on page 13 lines 310–316 in the main text, and the relevant data was presented in new Supplementary Fig. 17.

> *(10) The Methods section: a more detailed description of the experimental procedures involving HIV p24 and SARS-CoV-2 should be included.*

We thank the reviewer for pointing out this weakness.

In the revised manuscript, we have provided further details of the relevant experimental procedures in the Materials and Methods part, on page 21, lines 507–517.

> ***Reviewer #3 (Public review):***
>
> *Strengths:*
>
> *The core strength of this study lies in its innovative demonstration that an engineered sACE2-Fc fusion redirects virus-decoy complexes to Fc-mediated phagocytosis and lysosomal clearance in macrophages, revealing a distinct antiviral mechanism beyond traditional neutralization. Its complete prophylactic protection in animal models and precise targeting of airway phagocytes establish a novel therapeutic paradigm against SARS-CoV-2 variants and future respiratory viruses.*

We thank the reviewer for his recognition and positive comments on our study.

> *Weaknesses:*
>
> *The study attributes complete antiviral protection to Fc-mediated phagocytic clearance, a central claim that requires more rigorous experimental validation. The observation that abrogating Fc functions compromises protection could be confounded by potential alterations in the protein's stability, half-life, or overall structure. To firmly establish this*

> *mechanism, it is crucial to include a control molecule with a mutated Fc region that lacks FcγR binding while preserving the Fc structure itself. Without this critical control, the conclusion that phagocytic clearance is the primary mechanism remains inadequately supported.*

We thank the reviewer for his insightful comments and suggestions.

The L234A/L235A mutations in human IgG1 Fc region are most widely used to abolish its FcγR binding and Fc effector functions [13]. In this study, we have used B5-D3-LALA in the *in vivo* infection experiments in K18-hACE2 mice, as the control molecule that lacks FcγR binding while preserving the Fc structure (Figure 3, 4).

To address the reviewer's concern, we further performed new analysis comparing the efficiencies of different versions of B5-D3 in mediating pseudovirus uptake in THP-1-derived macrophages. In this test, B5-D3-LALA and B5-D3 were examined side-by-side to address the role of Fc effector functions in the phagocytosis process. Meanwhile, IgG1 isotype control was examined to address ACE2-specific effect. Indeed, we detected significant reduction of pseudovirus uptake based on p24 signal, in the B5D3-LALA treated samples compared to those receiving B5-D3. This decreased pseudoviral uptake correlated with the loss of Fc-mediated effector functions in B5-D3-LALA, indicating the involvement of Fc functions in efficient macrophage uptake of B5-D3-virus complex.

In the revised manuscript, we have included these results on page 13 lines 310–316 in the main text and presented relevant data in Supplementary Fig. 17.

> *The strategy of deliberately targeting virus-decoy complexes to phagocytes via Fc receptors inherently raises the question of Antibody-Dependent Enhancement (ADE) of disease. While the authors demonstrate a lack of productive infection in macrophages, this only addresses one facet of ADE. The risk of Fc-mediated exacerbation of inflammation (ADE) remains a critical concern. The manuscript would be significantly strengthened by a direct discussion of this risk and by including data, such as cytokine profiling from treated macrophages, to more comprehensively address the safety profile of this approach.*

(1) We thank the reviewer for his insightful comments and suggestions regarding the ADE issue.

Indeed, Antibody-Dependent Enhancement (ADE) of viral infection is a critical concern when developing the ACE2 decoy strategy. In this study, we have carefully examined the relevant risk based on our data from various *in vitro* and *in vivo* assays.

In our *in vivo* infection experiments, all B5-D3 prophylaxis and treatment groups, regardless of the administration times and routes, showed improved outcomes like less body-weight loss and better survival, compared to the PBS control groups (Figure 2). None of these treatment groups demonstrated worsened infections, indicating that ADE phenomenon was not occurring or did not play a major role during the B5-D3 treatments. Instead, moderate immune activation was observed in the lung of B5-D3 treated mice, which occurred much earlier but was milder compared to that in the PBS groups, and may reflect responses that lead to the efficient early clearance of viruses without observable symptoms (Figure 3 and 4).

In our *in vitro* assays shown in Figure 6, B5-D3 treatments in epithelial or non-immune cell models (hACE2-Galu-3 and hACE2-293T) significantly blocked the entry of pseudovirus into cells and yielded much reduced luciferase signals (Figure 6d–g). Whereas in the THP-1-derived macrophages, although the presence of B5-D3 largely enhanced the entry of SARS-CoV-2 pseudovirus into cells (Figure 6a,b), it did not result in active infection and produced no luciferase signal (Figure 6g). These results were robustly reproducible, indicating that pseudoviruses did not successfully release its genome RNA and viral proteins (like RTase and

integrases) after entering macrophages. Instead, colocalization analysis of p24 (pseudoviruses), sACE2-Fc (B5-D3), and LAMP1 (lysosome) signals suggested probability of pseudovirus degradation in endosomes/lysosomes after cell entry (Figure 6a,c). Consistently, examination of the macrophages that had taken up pseudovirus showed that the Spike (S) proteins from the pseudovirus particles were not cleaved to release S2' fragment at a distinct smaller size (Figure 6h). As the cleavage of S protein in host cells is critical for effective membrane fusion, it is essential and regarded as hallmark for successful viral entry and escape from endosome. Collectively, these data consistently indicated that the SARS-CoV-2 pseudoviruses were degraded directly in lysosomes after entering macrophages, showing no sign of ADE.

(2) We thank the reviewer for his valuable suggestion and have performed RNA-seq analysis to profile immune responses in the treated macrophages.

We performed RNA-Seq analysis to investigate major transcriptional changes in THP-1-derived macrophages after the pseudovirus infection, with or without B5-D3 treatments. Although no individual genes fulfilled the cutoff threshold of significant up-/down-regulation, we observed antiviral responses in the pseodovirus-B5-D3 treated samples by GSEA (new Supplementary Fig. 18). This observation indicated that the B5-D3 treatment and subsequent cell-entry of pseudovirusB5-D3 complexes into macrophages induced immune activation at moderate levels, but not evoking strong immune responses that can be harmful to the host.

In the revised manuscript, we have included the new RNA-seq analysis results on macrophage infection tests on page 13 lines 317–322 and page 14 lines 323–325 in the main text and presented the relevant data in the new Supplementary Fig. 18. Furthermore, we agree that ADE is a critical issue and have further enriched our discussion on page 17 lines 415–417, to emphasize that the risk for ADE should be thoroughly evaluated to further develop the decoy strategy for human use.

> *The exclusive use of the K18-hACE2 mouse model, which exhibits severe disease, limits the generalizability of the findings. The "complete protection" observed may not translate to models with more robust and naturalistic immune responses or to human physiology.*

We thank the reviewer for pointing out the limitation of the mouse model used.

(1) Given that wild type mice are not susceptible to SARS and SARS-CoV-2 infection, transgenic mice have been generated to express hACE2, through various designs and strategies, serving as models for viral infection and drug development. However, many of these hACE2 transgenic mouse models exhibit mild infections due to moderate hACE2 levels, failing to develop the severity observed in SARS and COVID patients [14].

(2) The K18-hACE2 transgenic mouse line (B6. Cg-Tg(K18-ACE2)2Prlmn/J, Jackson Laboratory) used in our study carries multiple copies of K18-hACE2 transgene cassette [15]. Compared to other hACE2 transgenic mouse models, this K18-hACE2 line shows higher expression of hACE2 in airway and other epithelia and supports severer infections by both SARS and SARS-CoV2 viruses, successfully causing lethality [16]. Hence, K18-hACE2 mice is a widely used model to study SARS and SARS-CoV2 virus infections and drug developments.

(3) We agree that K18-hACE2 mice is a relatively weak transgenic line with poor productivity. However, it demonstrates best susceptibility to SARS-CoV-2 infection among established mouse models. In this study, we observed robust responses to SARS-CoV-2 infection in both aged and young cohorts, with all infected mice consistently demonstrating significant body weight loss during 4 dpi to 7 dpi (the PBS groups in Figure 2b, g)

We agree with the reviewer that it would be more convincing to assess the efficacy of B5-D3 using additional animal models. However, we have some reservations about the importance of these additional tests. First, the generality of ACE2-Fc decoy concept and its efficacy have

been reported in other studies using various models [17,18]. Moreover, different transgenic mice or animal models exhibit distinct kinetics in the pathogenesis process and immune responses to SAS-CoV-2 infections, which differ from that in human patients at varied aspects. Hence, given the limited capacity of animal facility, we chose to focus on the K18-hACE2 mice that have demonstrated most robust and convincing infection data, to investigate the potential of B5-D3 administered through various strategies as well as the underlying mechanisms for the full protection observed in IN prophylaxis.

In the revised manuscript, we have further enriched our discussion regarding this limitation, on page 17 lines 417–422.

> *Furthermore, the lack of data on circulating SARS-CoV-2 variants is a concern*

We thank the reviewer for his valuable comment.

In this study, we have demonstrated the viral neutralization capacity of B5-D3, as a representative of the enhanced sACE2 decoy, using multiple pseudoviruses and authentic SARS-CoV-2, which collectively covered eleven variants (up to Omicron strains). Our results from both *in vitro* neutralization and PRNT experiments confirmed the robust resilience of B5-D3 against viral evolution (Figure 1c–g). This observation aligns well with other studies and is broadly supported by various investigations, as was pointed out below by the reviewer.

Furthermore, studies on viral evolution have observed a robust trend that later-emerging SARS-CoV-2 variants exhibit a higher affinity for the ACE2 receptor, enhancing their infectivity and transmissibility [19]. Therefore, it is unlikely for a newly emerged SARS-CoV-2 variant to escape from B5-D3mediated neutralization.

Collectively, all evidence consistently supports the principle of decoy design, B5-D3 (or other effective ACE2 decoys) possess the intrinsic ability to neutralize new circulating SARS-CoV-2 variants, as long as the virus variants rely on ACE2 receptor for cell entry. Hence, although further tests on circulating viral variants would add strengths to our study, the significance of this additional data may be limited.

In the revised manuscript, we have further addressed this concern in the discussion, on page 16 lines 394–397.

> *The concept of sACE2-Fc fusion proteins as decoy receptors is not novel, and numerous similar constructs have been previously reported. The manuscript would benefit from a clearer demonstration of how the optimized B5-D3 mutant represents a significant advance over existing sACE2-Fc designs.*

We thank the reviewer for his valuable comments.

Indeed, previous research has reported multiple ACE2 mutations to enhance its binding to spike proteins and neutralization against SARS-CoV-2. However, combining ACE2 mutations based on *in silico* predictions to both enhance spike binding and eliminate the ACE2 enzymatic activity resulted in accumulated burdens. For instance, ACE2 decoy candidates with up to five mutations like K31F/N33D/H34S/E35Q/H345L [8] and L79F/M82Y/Q325Y/H374A/H378A [12] have demonstrated excellent potency to neutralize SARS-CoV-2 in both *in vitro* and *in vivo* assays. However, the extensive mutations could be associated with structural instability and reduced production efficiency [8,12]. Furthermore, the high mutation loads increase risks for immunogenicity, which is a critical issue in future clinical applications. Corroboratively, Urano et al. detected *in vitro* T cell stimulation elicited by the L79F mutation, whereas the T92Q mutation (included in our decoy design) showed much lower immunogenicity and enhanced spike binding affinity [20].

In our ACE2 decoy design, we incorporated only two mutations (like T92Q and H374N in B5-D3) to enhance neutralization potency while eliminating enzymatic activity, resulting in simplest ACE2 mutants desired for engineering enhanced decoy. B5-D3, as one representative, not only exhibited minimal mutation-related risks (Supplementary Fig. 2i) but also top-level neutralization potencies among all candidate mutants tested (Figure 1, Supplementary Fig. 2f,g and Supplementary Fig. 3). To further address the safety of B5-D3 for *in vivo* use, we have performed prolonged *in vivo* overexpression of B5-D3 ACE2 decoy through AAV delivery in immune-competent K18-hACE2 mice, which indeed showed no sign of RAS disturbance or immune infiltration causing tissue damage. (In the revise manuscript, we have included these new results on page 5 lines 118–122 and page 6 lines 123–135 in the main text and presented the data in new Supplementary Fig. 4).

Therefore, instead of demonstrating advantage over existing sACE2-Fc designs, our study used the optimized B5-D3 as a representative ACE2 decoy of top performers, to systematically examined various administration strategies as well as the underlying mechanisms for the full protection observed in IN prophylaxis. Aligned with this effort, our study identified 6-hours IN prophylaxis as the most effective regimen to confer complete protection against SARS-CoV-2 infection in K18-hACE2 mice. Further investigation through transcriptomics, bio-distribution, and phagocytosis analysis revealed that IN-delivered B5-D3 not only neutralizes viruses but also engaged airway phagocytes to promote early viral clearance and host immune activation, uncovering a distinct antiviral mechanism for the universal “decoy strategy” to combat unknown air-borne respiratory virus in the future.

In the revised manuscript, we have further clarified our focus on using B5-D3 as a “representative” of ACE2 decoy on page 4 line 84, page 5 line 109, page 14 line 333, and page 15 line 360.

> *A direct comparative analysis with previously published benchmarks, particularly in terms of neutralizing potency, Fc effector function strength, and in vivo efficacy, is necessary to establish the incremental value and novelty of this specific agent.*

We thank the reviewer for his valuable comments.

Indeed, our study has aimed to address this concern and made partial progress through *in vitro* neutralization assays (Figure 1b and Supplementary Fig. 2c,d,f,g). Our results from the limited yet meaningful comparisons with the sACE2 lacking Fc domain and selected sACE2-Fc mutants published/proposed previously clearly demonstrated “substantial enhancement through Fc-fusion” (Supplementary Fig. 1d) and modest improvement from protein mutagenesis at ACE2-Spike interaction interface” (Figure 1b and Supplementary Fig. 2c,d,f,g).

Based on the results from our various neutralization assays, we chose B5-D3 as a representative of enhanced decoy for *in vivo* infection, which identified 6-hours IN prophylaxis to confer complete protection against infection, demonstrating significant impact of administration strategies on *in vivo* efficacy of B5-D3 (Figure 2). Subsequent analysis further uncovered intriguing phenomena regarding the cellular distribution of IN-administered B5-D3 and the early immune activation triggered in the lung, which underlies the full protection by IN prophylaxis and represents an important novelty of this study.

We agree with the reviewer that further analysis with additional benchmark versions would enhance the value of this study, but we have reservation regarding the importance. To enhance clarity, in the revised manuscript, we have further emphasized our study focus on using B5-D3 as a representative ACE2 decoy throughout the text and enriched the discussion on page 15 line 348–365.

References

(1) Ku Z, Xie X, Hinton PR, Liu X, Ye X, Muruato AE, Ng DC, Biswas S, Zou J, Liu Y, Pandya D, Menachery VD, Rahman S, Cao Y-A, Deng H, Xiong W, Carlin KB, Liu J, Su H, Haanes EJ, Keyt BA, Zhang N, Carroll SF, Shi P-Y & An Z. Nasal delivery of an IgM offers broad protection from SARS-CoV-2 variants. Nature 595, 718-723 (2021).

(2) Liu J, Mao F, Chen J, Lu S, Qi Y, Sun Y, Fang L, Yeung ML, Liu C, Yu G, Li G, Liu X, Yao Y, Huang P, Hao D, Liu Z, Ding Y, Liu H, Yang F, Chen P, Sa R, Sheng Y, Tian X, Peng R, Li X, Luo J, Cheng Y, Zheng Y, Lin Y, Song R, Jin R, Huang B, Choe H, Farzan M, Yuen KY, Tan W, Peng X, Sui J & Li W. An IgM-like inhalable ACE2 fusion protein broadly neutralizes SARSCoV-2 variants. Nat Commun 14, 5191 (2023).

(3) Guo H, Cho B, Hinton PR, He S, Yu Y, Ramesh AK, Sivaccumar JP, Ku Z, Campo K, Holland S, Sachdeva S, Mensch C, Dawod M, Whitaker A, Eisenhauer P, Falcone A, Honce R, Botten JW, Carroll SF, Keyt BA, Womack AW, Strohl WR, Xu K, Zhang N, An Z, Ha S, Shiver JW & Fu T-M. An ACE2 decamer viral trap as a durable intervention solution for current and future SARS-CoV. Emerging Microbes & Infections 12, 2275598 (2023).

(4) Keyt BA, Baliga R, Sinclair AM, Carroll SF & Peterson MS. Structure, Function, and Therapeutic Use of IgM Antibodies. Antibodies 9, 53 (2020).

(5) Chan KK, Dorosky D, Sharma P, Abbasi SA, Dye JM, Kranz DM, Herbert AS & Procko E. Engineering human ACE2 to optimize binding to the spike protein of SARS coronavirus 2. Science 369, 1261-1265 (2020).

(6) Guy JL, Jackson RM, Jensen HA, Hooper NM & Turner AJ. Identification of critical active-site residues in angiotensin-converting enzyme-2 (ACE2) by site-directed mutagenesis. The FEBS Journal 272, 3512-3520 (2005).

(7) Payandeh Z, Rahbar MR, Jahangiri A, Hashemi ZS, Zakeri A, Jafarisani M, Rasaee MJ & Khalili S. Design of an engineered ACE2 as a novel therapeutics against COVID-19. Journal of Theoretical Biology 505, 110425 (2020).

(8) Glasgow A, Glasgow J, Limonta D, Solomon P, Lui I, Zhang Y, Nix MA, Rettko NJ, Zha S, Yamin R, Kao K, Rosenberg OS, Ravetch JV, Wiita AP, Leung KK, Lim SA, Zhou XX, Hobman TC, Kortemme T & Wells JA. Engineered ACE2 receptor traps potently neutralize SARS-CoV2. Proceedings of the National Academy of Sciences 117, 28046-28055 (2020).

(9) Lei C, Qian K, Li T, Zhang S, Fu W, Ding M & Hu S. Neutralization of SARS-CoV-2 spike pseudotyped virus by recombinant ACE2-Ig. Nature Communications 11, 2070 (2020).

(10) Maciuba S, Bowden GD, Stratton HJ, Wisniewski K, Schteingart CD, Almagro JC, Valadon P, Lowitz J, Glaser SM, Lee G, Dolatyari M, Navratilova E, Porreca F & Riviere PJM. Discovery and characterization of prolactin neutralizing monoclonal antibodies for the treatment of female-prevalent pain disorders. MAbs 15, 2254676 (2023).

(11) Dwivedi V, Shivanna V, Gautam S, Delgado J, Hicks A, Argonza M, Meredith R, Turner J, Martinez-Sobrido L, Torrelles JB & Kulkarni V. Age associated susceptibility to SARS-CoV-2 infection in the K18-hACE2 transgenic mouse model. Geroscience 46, 2901-2913 (2024).

(12) Chen Y, Sun L, Ullah I, Beaudoin-Bussières G, Anand SP, Hederman AP, Tolbert WD, Sherburn R, Nguyen DN, Marchitto L, Ding S, Wu D, Luo Y, Gottumukkala S, Moran S, Kumar P, Piszczek G, Mothes W, Ackerman ME, Finzi A, Uchil PD, Gonzalez FJ & Pazgier M. Engineered ACE2-Fc counters murine lethal SARS-CoV-2 infection through direct neutralization and Fc-effector activities. Science Advances 8, eabn4188 (2022).

(13) Lund J, Winter G, Jones PT, Pound JD, Tanaka T, Walker MR, Artymiuk PJ, Arata Y, Burton DR, Jefferis R & Woof JM. Human Fc gamma RI and Fc gamma RII interact with distinct but

overlapping sites on human IgG. The Journal of Immunology 147, 2657-2662 (1991).

(14) Lutz C, Maher L, Lee C & Kang W. COVID-19 preclinical models: human angiotensinconverting enzyme 2 transgenic mice. Hum Genomics 14, 20 (2020).

(15) McCray PB, Pewe L, Wohlford-Lenane C, Hickey M, Manzel L, Shi L, Netland J, Jia HP, Halabi C, Sigmund CD, Meyerholz DK, Kirby P, Look DC & Perlman S. Lethal Infection of K18hACE2 Mice Infected with Severe Acute Respiratory Syndrome Coronavirus. Journal of Virology 81, 813-821 (2007).

(16) Oladunni FS, Park JG, Pino PA, Gonzalez O, Akhter A, Allue-Guardia A, Olmo-Fontanez A, Gautam S, Garcia-Vilanova A, Ye C, Chiem K, Headley C, Dwivedi V, Parodi LM, Alfson KJ, Staples HM, Schami A, Garcia JI, Whigham A, Platt RN, 2nd, Gazi M, Martinez J, Chuba C, Earley S, Rodriguez OH, Mdaki SD, Kavelish KN, Escalona R, Hallam CRA, Christie C, Patterson JL, Anderson TJC, Carrion R, Jr., Dick EJ, Jr., Hall-Ursone S, Schlesinger LS, Alvarez X, Kaushal D, Giavedoni LD, Turner J, Martinez-Sobrido L & Torrelles JB. Lethality of SARS-CoV-2 infection in K18 human angiotensin-converting enzyme 2 transgenic mice. Nat Commun 11, 6122 (2020).

(17) Urano E, Itoh Y, Suzuki T, Sasaki T, Kishikawa JI, Akamatsu K, Higuchi Y, Sakai Y, Okamura T, Mitoma S, Sugihara F, Takada A, Kimura M, Nakao S, Hirose M, Sasaki T, Koketsu R, Tsuji S, Yanagida S, Shioda T, Hara E, Matoba S, Matsuura Y, Kanda Y, Arase H, Okada M, Takagi J, Kato T, Hoshino A, Yasutomi Y, Saito A & Okamoto T. An inhaled ACE2 decoy confers protection against SARS-CoV-2 infection in preclinical models. Sci Transl Med 15, eadi2623 (2023).

(18) Higuchi Y, Suzuki T, Arimori T, Ikemura N, Mihara E, Kirita Y, Ohgitani E, Mazda O, Motooka D, Nakamura S, Sakai Y, Itoh Y, Sugihara F, Matsuura Y, Matoba S, Okamoto T, Takagi J & Hoshino A. Engineered ACE2 receptor therapy overcomes mutational escape of SARS-CoV-2. Nature Communications 12, 3802 (2021).

(19) Cho MJ, Been NR & Son H. From Alpha to Omicron: Structural Insights into SARS-CoV-2 RBD Evolution and ACE2 Binding. European Journal of Public Health 35(2025).

(20) Urano E, Itoh Y, Suzuki T, Sasaki T, Kishikawa J-i, Akamatsu K, Higuchi Y, Sakai Y, Okamura T, Mitoma S, Sugihara F, Takada A, Kimura M, Nakao S, Hirose M, Sasaki T, Koketsu R, Tsuji S, Yanagida S, Shioda T, Hara E, Matoba S, Matsuura Y, Kanda Y, Arase H, Okada M, Takagi J, Kato T, Hoshino A, Yasutomi Y, Saito A & Okamoto T. An inhaled ACE2 decoy confers protection against SARS-CoV-2 infection in preclinical models. Science Translational Medicine 15, eadi2623 (2023).

https://doi.org/10.7554/eLife.108883.2.sa0